ERDC/GSL TR-21-41

US Army Corps
of Engineers®
Engineer Research and
Development Center

Rapid Airfield Damage Recovery Program

Evaluation of Geocell-Reinforced Backfill for Airfield Pavement Repair

Lyan Garcia, Jay Rowland, and Jeb Tingle

December 2021

Geotechnical and Structures Laboratory

The U.S. Army Engineer Research and Development Center (ERDC) solves the nation's toughest engineering and environmental challenges. ERDC develops innovative solutions in civil and military engineering, geospatial sciences, water resources, and environmental sciences for the Army, the Department of Defense, civilian agencies, and our nation's public good. Find out more at www.erdc.usace.army.mil.

To search for other technical reports published by ERDC, visit the ERDC online library at https://erdclibrary.on.worldcat.org/discovery.

ERDC/GSL TR-21-41
December 2021

Evaluation of Geocell-Reinforced Backfill for Airfield Pavement Repair

Lyan Garcia, Jay Rowland, and Jeb Tingle

Geotechnical and Structures Laboratory
U.S. Army Engineer Research and Development Center
3909 Halls Ferry Road
Vicksburg, MS 39180-6199

Final report

Prepared for Air Force Civil Engineer Center
Panama City, FL 32403

Under Geocell TTP Refinement, Project Number 475573

Abstract

After an airfield has been attacked, temporary airfield pavement repairs should be accomplished quickly to restore flight operations. Often, the repairs are made with inadequate materials and insufficient manpower due to limited available resources. Legacy airfield damage repair (ADR) methods for repairing bomb damage consist of using bomb damage debris to fill the crater, followed by placement of crushed stone or rapid-setting flowable fill backfill with a foreign object debris (FOD) cover. While these backfill methods have provided successful results, they are heavily dependent on specific material and equipment resources that are not always readily available. Under emergency conditions, it is desirable to reduce the logistical burden while providing a suitable repair, especially in areas with weak subgrades. Geocells are cellular confinement systems of interconnected cells that can be used to reinforce geotechnical materials. The primary benefit of geocells is that lower quality backfill materials can be used instead of crushed stone to provide a temporary repair. This report summarizes a series of laboratory and field experiments performed to evaluate different geocell materials and geometries in combinations with a variety of soils to verify their effectiveness at supporting heavy aircraft loads. Results provide specific recommendations for using geocell technology for backfill reinforcement for emergency airfield repairs.

Contents

Figures and Tables

Figures

Tables

Preface

This study was conducted for the U.S. Air Force Civil Engineer Center (AFCEC) under the Rapid Airfield Damage Recovery Research and Development Program, Project Number 475573. The AFCEC technical monitor was Dr. Robert A. Diltz. The Program Manager was Mr. Jeb S. Tingle, Senior Scientific Technical Manager.

This work was performed by the Airfields and Pavements Branch (GMA) of the Engineering Systems and Materials Division (GM), U.S. Army Engineer Research and Development Center, Geotechnical and Structures Laboratory (ERDC-GSL). At the time of publication, Ms. Anna Jordan was Chief, GMA; Mr. Justin S. Strickler was Chief, GM; and Mr. R. Nicholas Boone, GZT, was the Technical Director for Force Projection and Maneuver Support. Mr. Charles W. Ertle II was Deputy Director of ERDC-GSL, and Mr. Bartley P. Durst was the Director.

COL Teresa A. Schlosser was the Commander of ERDC, and Dr. David W. Pittman was the Director.

1 Introduction

1.1 Airfield damage repair

The airfield damage repair (ADR) process consists of engineer personnel activities in response to an attack on an airbase to provide adequate launch and recovery surfaces for the mission aircraft. Although ADR criteria are based on repairing airfields in friendly territory, recent military operations required repairing airbases occupied previously by hostile forces and damaged during forcible entry or purposely sabotaged by departing forces. Legacy ADR methods for repairing bomb damage consist of using debris to fill the crater, followed by placement of crushed stone backfill with a foreign object debris (FOD) cover.

The U.S. Army Engineer Research and Development Center's (ERDC) efforts more recently have been dedicated to address the operational limitations of legacy repair methods. Research was conducted to develop the capability to return damaged runways to full operational sortie production in less than 8 hr. Evaluations included new materials; tactics, techniques, and procedures (TTPs); and prototype equipment for rapid automated airfield damage assessment and crater repair (Tingle et al. 2009). Multiple operational utility assessments (OUAs) were conducted to demonstrate the updated ADR methods and to collect feedback from the end users for further refinement as part of the Critical Runway AssessmenT and Repair (CRATR) Joint Capabilities Technology Demonstration (JCTD). Since the CRATR JCTD, multiple other troop and full-scale tests have been conducted to address other gaps identified within the scope of the Rapid Airfield Damage Recovery (RADR) modernization program. The RADR program is focused on refining techniques and reducing the logistical footprint of the ADR process.

1.2 RADR modernization program

The crater repair process developed during the CRATR JCTD and further refined during the RADR modernization program is well-documented in many references (e.g., Bell et al. 2013; Priddy et al. 2013; Edwards et al. 2013; Carruth et al. 2015). First, large debris is removed with compact track loaders and large front-end loaders. Next, the stanchion method (USAF 1992) is used to mark the extent of upheaval before a square repair area on

the pavement is marked. The marked area is then saw-cut, followed by breaking and removing the existing material with wheeled excavators.

Once the repair is excavated, it is backfilled, typically with rapid-setting flowable fill or compacted crushed stone. The main purpose of the backfill is to fill the void and provide enough support to the repair cap to withstand the loads from aircraft traffic. Rapid-setting flowable fill has proven to be the best backfill alternative for RADR. The repair is then capped with rapid-setting concrete by using the U.S. Air Force Simplified Volumetric Mixer or with recycled asphalt cookies by using a Bagela recycler and appropriate large pneumatic and steel-wheel compaction equipment.

While the current RADR crater repair method provides successful results, it is heavily dependent on specific material and equipment resources. Other repair alternatives are required in the event that large quantities of rapid-setting flowable fill and rapid-setting cement cannot be transported to the repair site. Backfill alternatives are not included in the TTPs.

1.3 Geocells for RADR

The concept of using sand-confinement systems, or geocells, as an expedient construction method for reinforcing pavement base courses above soft ground was first investigated by Webster and Alford (1978). The study focused on military truck traffic, and findings supported the use of geocells as a suitable construction technique where sand was readily available. Follow on investigations by Webster (1979; 1981) determined optimum geocell grid size (cell diameter and thickness/height), cell shape (see Figure 1-1), geocell material, and minimum surfacing requirements for handling over-the-shore military 5-ton truck operations. A geocell with a height of 8 in. was recommended, although a geocell with a height of 6 in. was recommended if the sand was well-graded. As cell area increased, the performance tended to decrease; thus, the authors recommended cell areas of 36 to 44 sq. in.

Figure 1-1. Hexagonal geocells (Webster 1981).

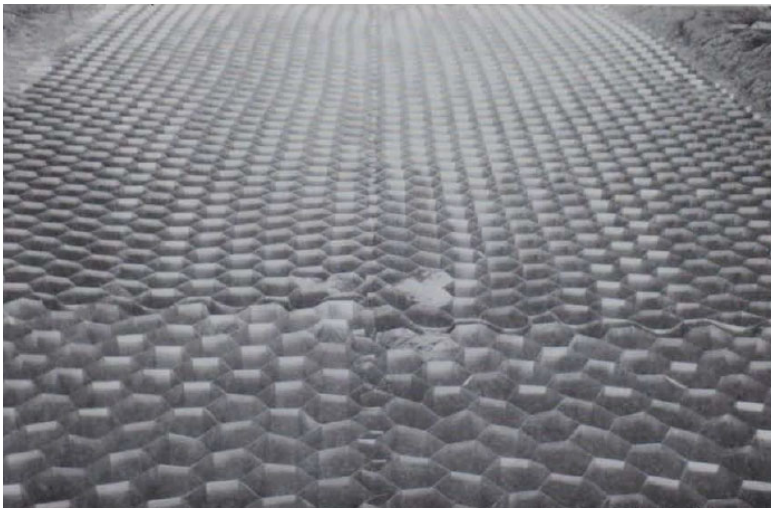

Among grid materials recommended for further evaluation were aluminum and plastic. Webster (1984; 1986) further refined the geocell technology into a high-density polyethylene (HDPE) grid that could be easily collapsed and then expanded on site to an area of approximately 8 ft by 20 ft of total panel size. HDPE strips were ultrasonically welded at intervals of 13 in.

In a program sponsored by the Waterways Experiment Station in Vicksburg, MS, geocells were demonstrated for military road construction and were ultimately proven as a practical solution for increasing the offload efficiency during over-the-shore operations. Webster (1986) published specifications for HDPE grid sections as a result of these demonstrations, and the geocell concept was commercialized with a product called “Geoweb.” At that point, however, geocells were still being evaluated for application in construction or repair of airfield pavements.

Read and Dukes (1988) investigated the use of geocells to reinforce the base course in bomb damage crater repairs to alleviate the requirement for high-quality, well-graded crushed stone. The repairs consisted of two layers of geocell-reinforced sand, i.e., 16-in.-total reinforced thickness, placed on a clay subgrade with a California bearing ratio (CBR) of 5. Each repair was surfaced with fiberglass matting and trafficked with a load cart simulating the F-15 aircraft, i.e., 355-psi tire, 30,600-lb wheel load. Nearly all deformation occurred in the sand grid layers that was attributed to compression of the sand fill, local shear within the cells, and lateral spreading of the grids. The authors

concluded that compaction was a major factor affecting performance and recommended a coarser sand (e.g., concrete sand.)

Since then, expedient airfield pavement repair with geocells has been established as a standard procedure with detailed methods included in the *Unified Facilities Criteria (UFC): Airfield Damage Repair* (UFC 3-270-07) (Department of Defense 2002). When surfaced with the recommended fiberglass FOD cover, the repair method is defined as an expedient repair and is approved for 100 C-130 operations on runways and taxiways. Geocell reinforcement is a useful alternative to traditional backfill methods such as crushed stone or rapid-setting flowable fill because lower quality backfill materials, i.e., indigenous materials, can be used to provide a temporary repair. The procedure requires two 8-in.-thick layers of geocell (Figure 1-2) filled with an indigenous material (ideally sand.) The geocell layers are placed perpendicular to each other over a minimum subgrade CBR of 4. Non-woven (NW) geotextile is placed between the two geocell layers. Geocell material and geometry specifications align with the properties of the Geoweb product.

Figure 1-2. Airfield pavement repair method using geocell reinforcement.

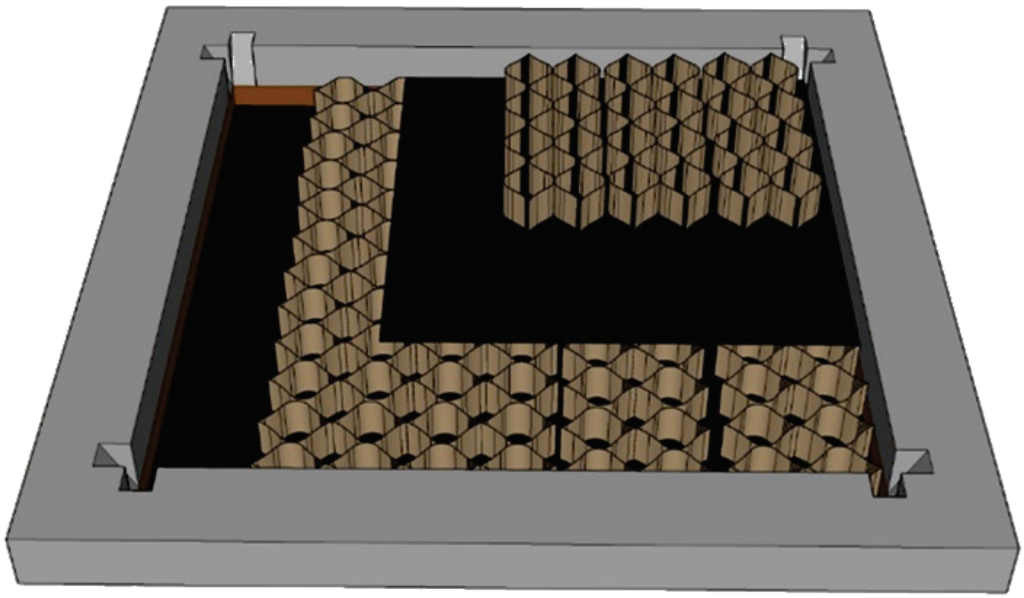

New geometries and geocell materials have been introduced commercially for several years, but research that specifically addressed the use of new products for airfield pavement repair was limited. To

address this capability gap, the ERDC in Vicksburg initiated a research program that aimed at evaluating new geocell products, materials, and geometries and their combination with good-quality and poor-quality fill materials. Information from the program were used to develop new product specifications and requirements for airfield pavement repair and, ideally, could be used to validate other geometries and materials that are commercially available for this application.

1.4 Objectives and approach

The objectives of this project were to perform (1) a market survey of traditional and new geocell products commercially available, (2) laboratory testing to characterize the different geocell materials and geometries, and (3) field experiments to determine how geocell material, geometry, and various backfill soil types could affect repair performance under simulated aircraft loads.

This report summarizes the findings and results of the objectives stated above. The project was carried out in a phased approach that started with a market survey, followed by a laboratory characterization program, and ended with a full-scale testing program that assisted with selection of optimal geocell geometry and geocell material. For the latter, simulated repairs were constructed at the ERDC and trafficked with simulated aircraft loading. Deformation was monitored to measure the performance of the repairs.

The organization of this report is as follows: Chapter 2 provides a summary of the test plan; Chapter 3 discusses the laboratory testing program and results; Chapter 4 provides information on materials and equipment used for the full-scale experiments; Chapter 5 describes the construction process of the repairs, trafficking with the load simulator, and data collection; Chapter 6 provides the results of the full-scale testing; and Chapter 7 summarizes conclusions from the testing program and recommendations for TTPs.

2 Test Plan and Layout

The experimental program consisted of laboratory-scale and full-scale experiments. The laboratory testing was carried out to characterize the different geocell materials and geometries and to relate the properties to full-scale performance. The data were used to develop product specifications for procurement. Details are provided in Chapter 3. The field experiments were performed at the Outdoor Pavement Testing Facility, East Campus of ERDC in Vicksburg.

Simulated craters, measuring 8.5-ft square, were cut and excavated in an existing concrete test area to a depth of at least 34 in. from the surface of the concrete. The existing concrete had a thickness of approximately 15 in. A layer of low-plasticity clay (CL) was placed and compacted at the bottom of the repairs to provide a consistent subgrade throughout the tests.

Five independent series of tests were conducted to evaluate specific objectives:

- Phase 1 – determine optimal length and width of individual cells in a geocell section
- Phase 2 – determine optimal geocell height
- Phase 3 – determine best performing geocell product/material
- Phase 4 – determine the benefit of geocells when filled with low- to high-quality backfill soils
- Phase 5 – validate the results of Phase 2.

In Phase 1, the same geocell material, geocell height, and backfill were used, while the geocell cell length and width were varied. In Phase 2, the geocell material, cell length and width, and backfill were the same, while the geocell height was varied. In Phase 3, the same geocell geometry and backfill were used, while the geocell material / manufacturer was varied. Finally, Phase 4 used the same geocell material and geometry, while the backfill was varied. Phase 5 was conducted to refine the results obtained from Phase 2, which is further explained in Chapter 6. For reference, geocell section length and width and individual cell length and width are defined in Figure 2-1. The test matrix is shown in Table 2-1.

Figure 2-1. Geocell length and width defined.

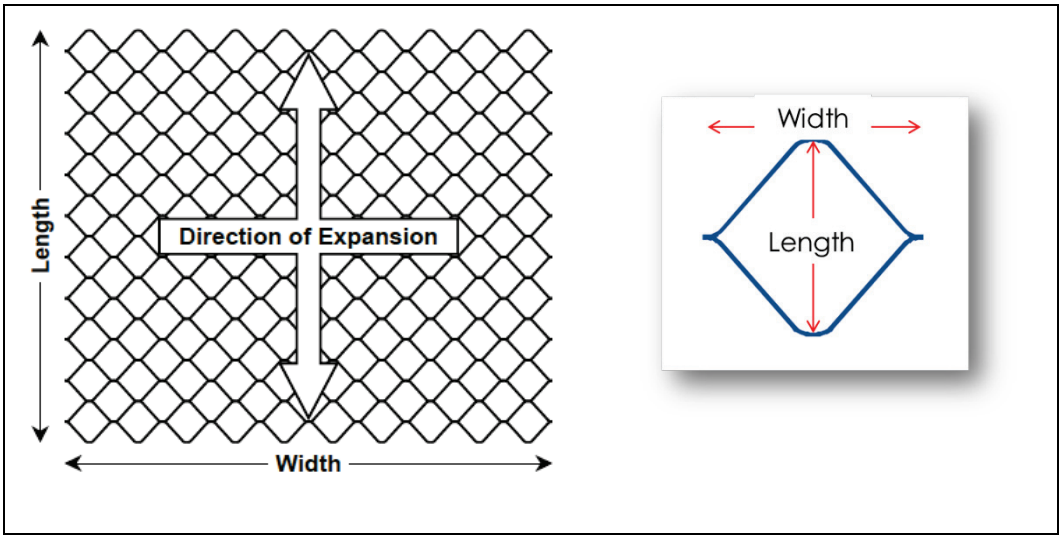

Phase 1 repairs were capped with 4 in. of crushed limestone. Phase 2 through 5 repairs were capped with a Fiberglass-Reinforced Polymer Panels (FRP) FOD cover. Simulated single-wheel C-17 aircraft traffic was applied to the finished repairs, and rut depth was monitored at different pass levels. The profile of each repair is shown in Figure 2-2 through Figure 2-4. The results of each phase were used to down-select specific variables, i.e., diameter, height, product/material, etc., for the following phase. For example, the optimal geocell length and width from Phase 1 were used as a controlled variable for testing different geocell heights in Phase 2. Since Presto-Geoweb, i.e., the original geocell product, has available historical data for comparison, it was used throughout all of the phases as a control variable.

Table 2-1. Field test matrix.

	Repair ID	Geocell Length [a] (in.)	Geocell Width [a] (in.)	Geocell Height (in.)	Manufacturer / Material	Model Number	Backfill [c]	Cap
Phase 1	Control (C-1)	N/A	N/A	N/A	N/A	N/A	SP	GP-GM
	1-A	8.8	10.2	8	Presto / HDPE	GW20V8		
	1-B	11.3	12.6			GW30V8		
	1-C	18.7	20			GW40V8		
Phase 2	Control (C-2)	N/A	N/A	N/A	N/A	N/A	SP	FRP
	2-A	8.8	10.2	8	Presto / HDPE	GW20V8		
	2-B			6		GW20V6		
	2-C			4		GW20V4		
Phase 3	3-A	8.8	10.2	8	PRS Geo-technologies / NPA [b]	Neoweb [356-200-D]	SP	FRP
	3-B				Geo Products/ HDPE	EnviroGrid [EGA208PT-27]		
	3-C				Presto / HDPE	Geoweb [GW20V8]		
	3-D	9	11		Typar / Non-woven PP/PE [d] geotextile	Typar 220/200		
Phase 4	4-A	8.8	10.2	8	Presto / HDPE	GW20V8	GP-GM	FRP
	4-B						SC (w/ gravel)	
	4-C						SP	
	4-D						GW	
	4-E						SC	
	4-F						CL-ML	
Phase 5	5-A	8.8	10.2	6	Presto / HDPE	GW20V6	SP	FRP
	5-B			8		GW20V8		

Notes: [a] dimension of an individual cell. These dimensions can vary depending on how much the geocell section/mattress is expanded.

[b] NPA = nano-polymeric alloy

[c] SP = poorly graded sand, GP-GM = poorly graded gravel with silt and sand, SC = clayey sand, GW = well-graded gravel with sand, CL-ML = silty clay

[d] PP / PE = polypropylene and polyethylene

Figure 2-2. Profiles of the Phase 1 and Phase 2 repairs (refer to Table 2-1).

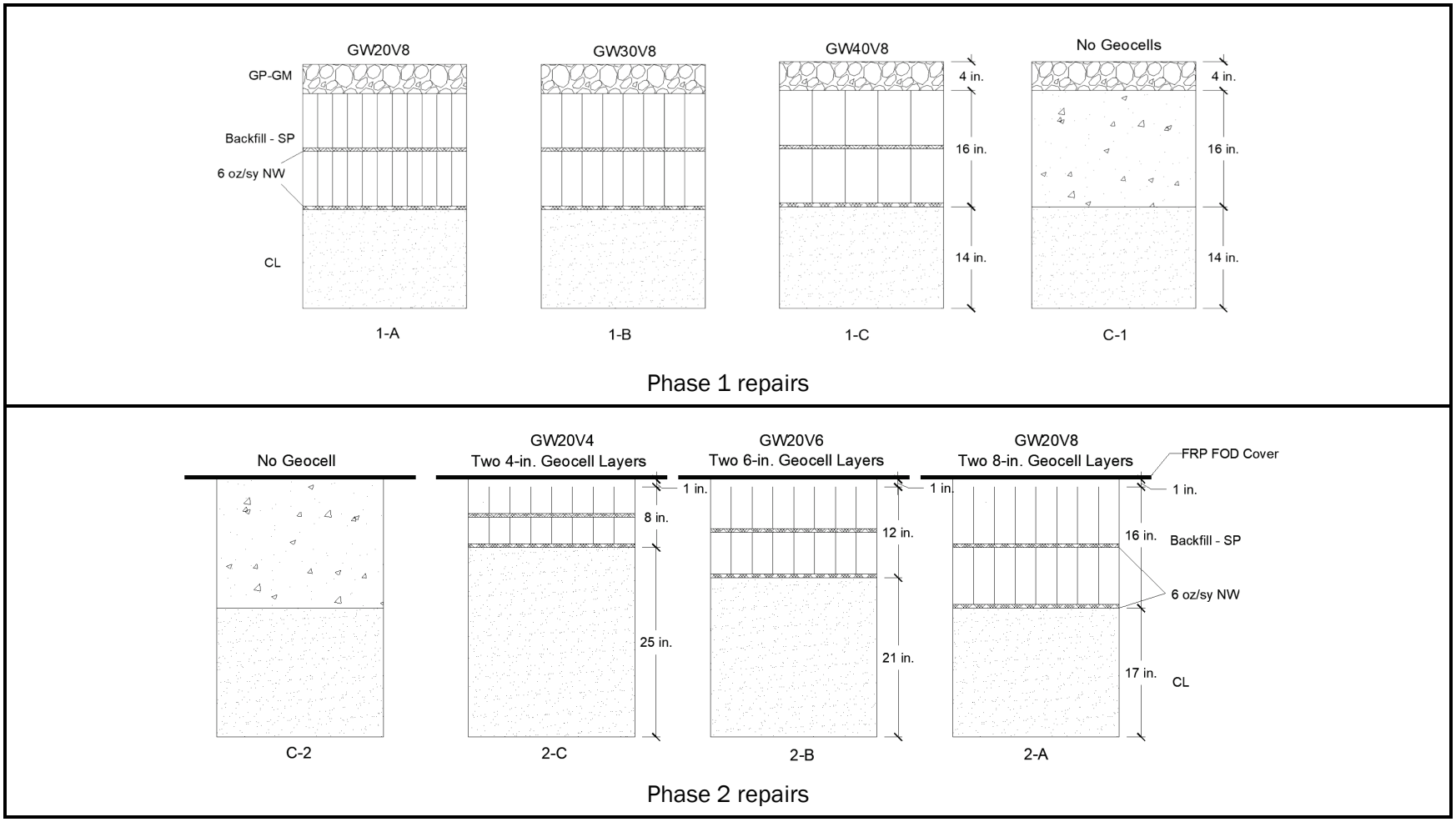

Figure 2-3. Profiles of the Phase 3 and Phase 4 repairs (refer to Table 2-1).

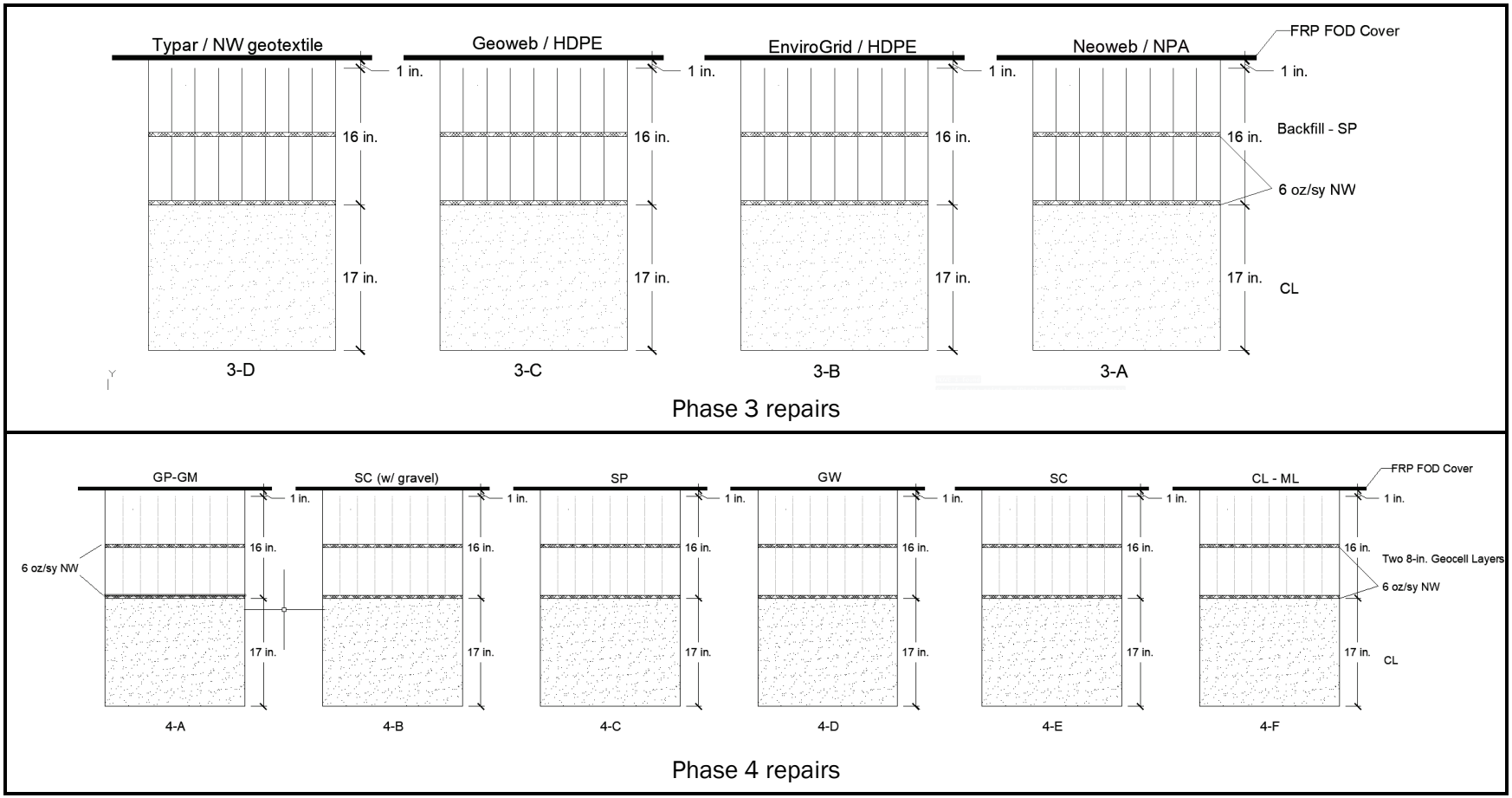

Figure 2-4. Profiles of the Phase 5 repairs (refer to Table 2-1).

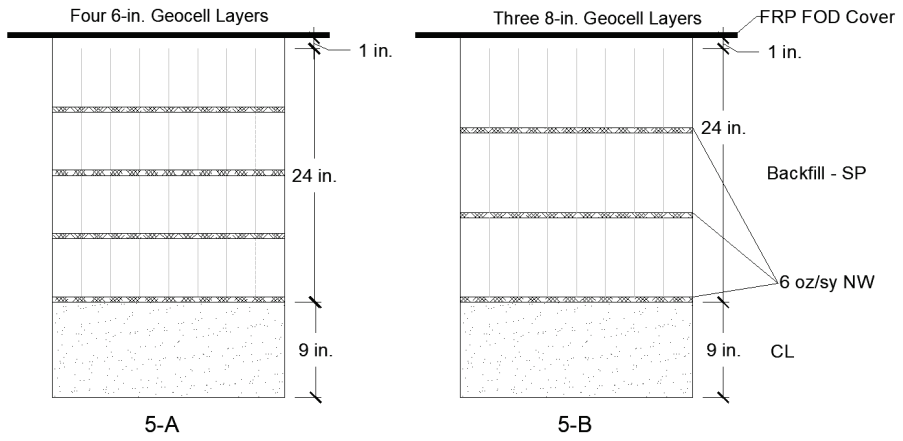

Phase 5 repairs

3 Laboratory Testing of Geocells

3.1 Description of geocell products

A market survey was conducted to identify products and geometries currently available commercially for procurement. The survey revealed a range of products, and the products from four vendors were selected to represent a lower-quality material, traditional material, and new material. Descriptions of these are provided in the following sections. Details on the products chosen for this testing program are shown in Table 3-1.

Table 3-1. Description of geocell products found in the market survey. (Note: not all products tested.)

Vendor	Product	Model Number	Material	Texture	% Perforation on Wall	Weld Type	Weld Spacing (in.)	Individual Cell Length (in.)	Individual Cell Width (in.)	Height (in.)
Presto Geosystems	Geoweb	GW20V4	HDPE	Perforated & textured	21.2	Ultrasonic	14	8.8	10.2	4
		GW20V6								6
		GW20V8								8
		GW30V8			16.8		17.5	11.3	12.6	8
		GW40V8			19.9		28	18.7	20	8
PRS Geo-technologies	Neoweb	330-200-D	Neoloy ; Novel Polymer alloy (NPA)	Perforated & textured	6-22	Ultrasonic	13	8.27	9.65	8
		356-100-D					14	8.82	10.24	4
		356-120-D								4.7
		356-150-D								6
		356-200-D								8
Geo Products	EnviroGrid	EGA204PT	HDPE	Perforated & textured	16 ± 3	Ultrasonic	14	8.8	10.2	4
		EGA206PT								6
		EGA208PT								8
		EGA308PT					17.5	11.3	12.6	8
		EGA408PT					28	18.7	20	8
Typar	GeoCell GS	220/200	Non-woven PP/PE bicomponent fiber geotextile	N/A	N/A	Epoxy	N/A	8.58	10.39	8
		250/150						10.43	11.081	6

Note: Data pulled from manufacturer data sheets.

3.1.1 Presto – Geoweb

The Geoweb product was developed in the 1980s and has been sold by Presto since the final concept was made commercial. The Geoweb geocells are made from HDPE strips that are ultrasonically welded together at intervals, depending on the desired nominal cell dimensions. They are available in different geometries and have the option of being perforated and textured, depending on the application. The Geoweb products used for these experiments were textured and perforated to allow the dissipation of pore pressures in individual cells. The sections were delivered collapsed, banded, and placed on a wooden pallet, as shown in Figure 3-1. An individual section measured about 12 ft x 0.5 ft when collapsed. When expanded, the width could range from 8 ft to 9 ft (Figure 3-2). Different lengths of sections were available. Cost varied, depending on the geocell height and the length of the section. For a section that expanded to 21 ft in length, the GW20V4 costs $225 ($1.24/ sq ft), the GW20V6 costs $338 ($1.87 / sq ft), and the GW20V8 costs $541 ($2.99 / sq ft), as of 2016.

Figure 3-1. Collapsed and banded Geoweb geocell section.

Figure 3-2. Collapsed and expanded Geoweb geocell section.

3.1.2 PRS Geo-technologies – Neoweb

One of the newest geocell products available on the market is a product manufactured by PRS Geo-technologies called Neoweb. The geocell material is a nano-polymeric alloy (NPA), also called Neoloy®, which is a composite alloy of polyester/polymaride nano-fibers dispersed in a polyethylene matrix. The Neoweb geocell line is offered in categories, i.e., A-D, according to the application profile, where Category A is offered for erosion control on slopes and Category D is offered for load support in airports, railways, and railroads. For this test program, Category D Neoweb was chosen; these were textured and perforated. Individual strips were ultrasonically welded at intervals to form the cellular confinement system. PRS Geo-technologies offered several more options for geocell geometry and color than other vendors. The tan color was chosen for testing (Figure 3-3). The sections were delivered collapsed and measured about the same dimensions as the Geoweb collapsed section. Neoweb geocells were ordered directly from the manufacturer, which is located in Israel. Currently, there are no distributors in the United States. Cost varied depending on the length of a section and the height of the geocell. A section of PRS-356-150-D (6-in. height) that expanded to about 24 ft costs $186, while a section of PRS-356-200-D (8-in. height) costs $256, as of 2016.

Figure 3-3. Neoweb geocell.

3.1.3 Geo Products – EnviroGrid

The product manufactured by Geo Products, EnviroGrid, is very similar to Geoweb in appearance. The EnviroGrid geocells are made from HDPE strips that are ultrasonically welded together at intervals, depending on the desired nominal cell dimensions. They are available in different

geometries and have the option of being perforated and textured, depending on the application. The products used for these experiments were textured and perforated. The sections were delivered collapsed and laid flat on a large wooden pallet. An individual section measured about 12 ft x 0.5 feet when collapsed. When expanded, the width could range from 8 ft to 9 ft. Different lengths of sections are available; standard panels are constructed so that the length of expansion is about 21 ft. Cost varied depending on the geocell height and the length of the section. For a section that expanded to 21 ft in length, the EGA204PT (4-in. height) costs $104 ($0.62/sq ft), the EGA206PT (6-in. height) costs $159 ($0.95/sq ft), and the EGA208PT (8-in. height) costs $216 ($1.29/sq ft), as of 2016.

3.1.4 Typar - GeoCell GS

Typar manufactures a different type of geocell product constructed from a permeable fabric. The product is called GeoCell GS but will be referred to as Typar for the remainder of this report to avoid confusion with other geocell products. The individual fabric strips are made from dark gray nonwoven polypropylene and polyethylene (PP/PE) bicomponent fiber and are joined by an epoxy to form the cellular confinement system (Figure 3-4). Two products with different geometries were chosen for these experiments (Table 3-1). The Typar geocells were also unique in that the geocell section could be expanded in the direction of the shorter dimension of the geocell section. The width of the Typar 250/150 geocell section (as defined in Figure 2-1) was 23 ft, and the length was 16 ft. For Typar 220/200, the section was 20 ft wide x 10 ft long. One section of Typar 250/150 costs $377 ($1.08/sq ft), and one section of Typar 220/100 costs $200 ($1.70/sq ft), as of 2016.

Figure 3-4. Typar geocell.

3.2 Laboratory testing program

The laboratory testing program was performed by an external, certified laboratory under contract number W912HZ-17-P-0035. The lab testing was performed to characterize the mechanical properties of the geocells and to use this information for developing product specifications. The test matrix for the laboratory testing program is shown in Table 3-2, and descriptions of the seam (or weld) testing methods are provided in the following paragraphs.

Table 3-2. Laboratory testing program for the geocell products.

Product	ASTM D 4355 (2014a)	ASTM D5321 (2014b)	ASTM D 4885 (2011a)	ASTM D 4595 (2011b)	Seam Peel Strength (Webster 1986)	Seam Shear Strength	Seam Splitting Strength
GW20V4			X		X	X	
GW20V6			X		X	X	
GW20V8	X	X	X		X	X	X
GW30V8							X
GW40V8							X
EGA204PT			X		X	X	
EGA206PT			X		X	X	
EGA208PT	X	X	X		X	X	X
EGA308PT							X
EGA408PT							X
Typar 250/150				X	X	X	X
Typar 220/200	X	X		X	X	X	X
330-200-D							X
356-100-D			X		X	X	
356-120-D			X		X	X	
356-150-D			X		X	X	
356-200-D	X	X	X		X	X	X

Notes:

ASTM D 4355 (2014a) – Standard Test Method for Deterioration of Geotextiles by Exposure to Light, Moisture, and Heat in a Xenon Arc-Type Apparatus

ASTM D 5321 (2014b) – Standard Test Method for Deterioration of Geotextiles by Exposure to Light, Moisture, and Heat in a Xenon Arc-Type Apparatus.The fill material was Ottawa sand.

ASTM D 4885 (2011a) – Standard Test Method for Determining Performance Strength of Geomembranes by the Wide Strip Tensile Method

ASTM D 4595 (2011b) – Standard Test Method for Tensile Properties of Geotextiles by the Wide-Width Strip Method

A schematic of the seam peel strength test is shown in Figure 3-5. According to ERDC GL-86-19 (Webster 1986), the samples should have a length of 4 in. on each side of the seam. Strain rate was 12 in. per minute (ipm).

Figure 3-5. Seam peel strength test (Webster 1986).

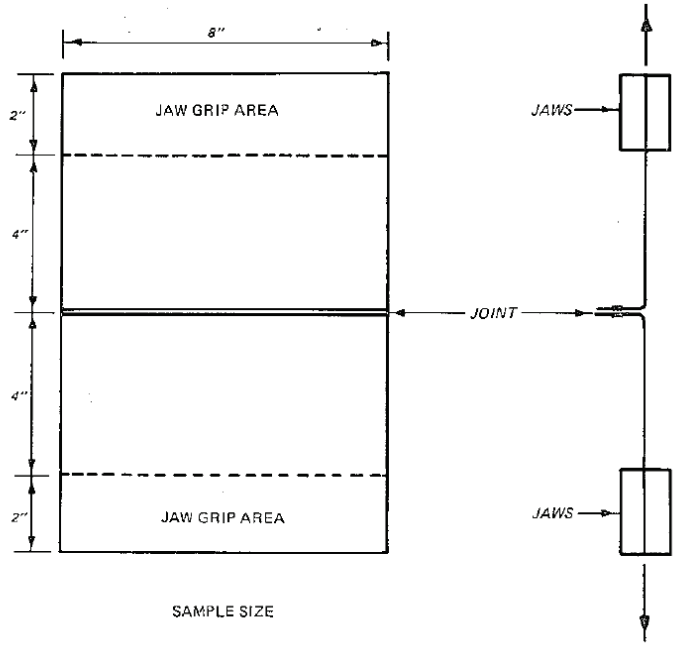

A schematic of the seam shear strength test is shown in Figure 3-6. ISO 13426-1 Method A (International Organization for Standardization 2003) was performed with the following modifications: (a) the strain rate was 12 ipm, and (b) the specimen length on each side of the seam was 4 in.

Figure 3-6. Seam shear strength test.

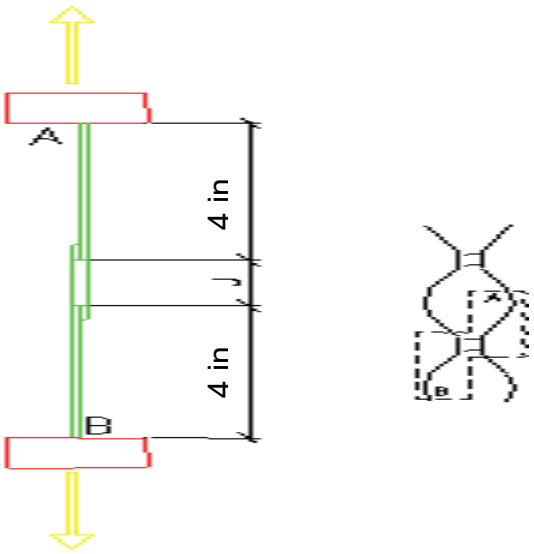

A schematic of the seam-splitting strength test is shown in Figure 3-7. ISO 13426-1 Method C (International Organization for Standardization 2003) was performed with the following modification: the strain rate was 12 ipm instead of 20% per minute. The splitting test required clamps that could hold the four strips in the same pattern and dimensions as they would be when the geocell panel is opened according to manufacturer recommendations (i.e., the specimen was placed in the clamps at the same cell aperture as indicated by the nominal cell size in Table 3-1).

Figure 3-7. Seam-splitting strength test.

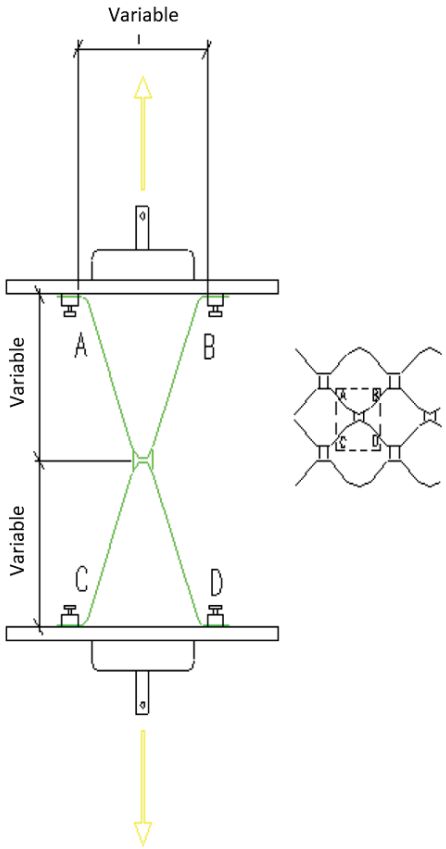

3.3 Laboratory testing results

Measured mechanical properties for the geocell products are shown in Table 3-3. The yield strength values in Table 3-3 for the Geoweb, EnviroGrid, and Neoweb product, is the point at which failure occurs in the force-elongation curve. The geosynthetic can continue to elongate at a reduced force per unit elongation until it eventually ruptures or breaks, which is why the elongation at yield and the break strength are also reported. The break strength can be higher or lower than the yield strength. For the textile product, Typar, the breaking toughness/strength is reported. This is a measure of the work-to-break per unit surface area of the material. The results according to ASTM D 5321 (2014b) are summarized in Appendix A.

The results showed that the yield strength and breaking strength for the Neoweb geocells was the highest, followed by EnviroGrid, and then Geoweb geocells. One factor that contributed to the behavior of Geoweb vs. EnviroGrid was the percent of wall perforation. While EnviroGrid and

Geoweb each consisted of the same material chemistry (HDPE), EnviroGrid had fewer wall perforations. The improved yield and breaking strength of the Neoweb geocells were associated with the inherent chemistry of the NPA material. However, EnviroGrid exhibited higher elongation at yield and at breaking than the Neoweb and Geoweb geocells. Typar geocells were made from geotextile, which allowed it to exhibit higher toughness than the NPA and HDPE products. UV resistance was highest for the Geoweb geocells. There was no clear trend that related yield and break strength to geocell height (geometry.)

Table 3-3. Mechanical properties of geocell products.

Manufacturer - Product		Presto - Geoweb			Geo Products - EnviroGrid			Typar – GeoCell GS		PRS Geo-technologies - Neoweb			
Model Number		GW20V4	GW20V6	GW20V8	EGA204PT	EGA206PT	EGA208PT	Typar 250/150	Typar 220/200	356-100-D	356-120-D	356-150-D	356-200-D
Yield Strength	Yield Strength (lb)	187.6	341.4	439.2	290.8	352.8	639.2	N/A	N/A	342.4	484.1	600	652
	Yield Strength (ppi)	46.9	56.9	54.9	72.7	58.8	79.9	N/A	N/A	85.6	103	100	81.5
	Yield Elongation (%)	8.44	8.6	9.1	19.3	12	24.5	N/A	N/A	11.5	11	11.8	11.9
UV Resistance	Yield Strength Retained (%)	Not tested	Not tested	95	Not tested	Not tested	94	Not tested	92	Not tested	Not tested	Not tested	92
	Elongation Retained (%)	Not tested	Not tested	98	Not tested	Not tested	92	Not tested	89	Not tested	Not tested	Not tested	88
Break Strength	Break Strength (lb)	174.8	298.8	392	278	336	614.4	768	1,112	274.8	376	483	592.8
	Break Strength (ppi)	43.7	49.8	49	69.5	56	76.8	128	139	68.7	80	80.5	74.1
	Break Elongation (%)	60.5	72.2	71.2	62.4	68.7	77.1	52.2	47	49	32.5	47	76

ppi = pounds per inch

Measured weld properties are shown in Table 3-4. Note that three failure modes are indicated: weld failure, material failure at the perforations, and material failure. Weld failure indicated that the specimen failed at the weld. Material failure at the perforations indicated that the specimen failed at the wall perforations. Material failure indicated that the specimen failed at another location that was not at the weld nor the

perforations. There was no clear trend that associated geocell height to peel and shear strength. Splitting strength did appear to increase with geocell diameter, but the failure modes were prevalent at the perforations. For example, the splitting strength was 96.8, 99.4, and 111.9 ppi for the EGA208PT, EGA308PT, and the EGA408PT, respectively. Failure modes tended to vary by test method and product. The Geoweb geocells mostly failed at the wall perforations. The EnviroGrid and Neoweb geocells failed at all three locations, but failure at the wall perforations was the most common. Typar geocells failed at the weld when subjected to the peel strength test but failed at the material when subjected to the shear and splitting strength tests.

It is desirable for failure to occur at the perforations or the material before failure occurs at the weld. Failure at the weld would yield failure of the system. The Geoweb geocells, therefore, exhibited better weld performance in terms of the dominating failure mode. However, because Geoweb geocells have more wall perforations than the other products (except Typar), the load at which failure occurred was generally lower.

Table 3-4. Weld properties of geocell products.

Manufacturer - Product	Model Number	Seam Peel Strength				Seam Shear Strength				Seam Splitting Strength		
		Peel Strength (lb)	Peel Strength (ppi)	Peel Efficiency (%)	Dominating Failure mode	Shear Strength (lb)	Shear Strength (ppi)	Shear Efficiency (%)	Dominating Failure Mode	Splitting Strength (lb)	Splitting Strength (ppi)	Dominating Failure Mode
Presto - Geoweb	GW20V4	208	52	111	2	211.6	52.9	113	2	—	—	—
	GW20V6	368.4	61.4	108	2	372.6	62.1	109	2	—	—	—
	GW20V8	477.6	59.7	109	2	466.4	58.3	106	2	632.8	79.1	2 & 3
	GW30V8	—	—	—	—	—	—	—	—	759.2	94.9	2
	GW40V8	—	—	—	—	—	—	—	—	759.2	94.9	2
Geo Products - EnviroGrid	EGA204PT	294	73.5	101	2	316.4	79.1	108	2	— [a]	— [a]	— [a]
	EGA206PT	275.4	45.9	78	1 & 3	389.4	64.9	110	2	— [a]	— [a]	— [a]
	EGA208PT	506.4	63.3	79	3	588	73.5	92	2	774.4	96.8	2 & 3
	EGA308PT	— [a]	— [a]	— [a]	— [a]	— [a]	— [a]	— [a]	— [a]	795.2	99.4	1&3
	EGA408PT	— [a]	— [a]	— [a]	— [a]	— [a]	— [a]	— [a]	— [a]	895.2	111.9	2
Typar – GeoCell GS	Typar 250/150	283.8	47.3	37	1	726	121	95	3	725	120.9	3
	Typar 220/200	301.6	37.7	27	1	1136	142	103	3	816	102	3
PRS Geo-technologies - Neoweb	356-100-D	223.6	55.9	65	3	400	100	117	2	— [a]	— [a]	— [a]
	356-120-D	263.2	56	54	1&3	535.8	114	110	2	— [a]	— [a]	— [a]
	356-150-D	190.2	31.7	32	1	708	118	118	2	— [a]	— [a]	— [a]
	356-200-D	640.8	80.1	98	3	694.4	86.8	106	2	952	119	2
	330-200-D	— [a]	— [a]	— [a]	— [a]	— [a]	— [a]	— [a]	— [a]	832	104	3

ppi = pounds per inch

[a] = Not tested

Dominating Failure Modes:

1 –Weld Failure

2 –Material Failure at Perforation

3 –Material Failure

4 Materials and Equipment

This chapter discusses the properties of the materials and equipment used for construction of the simulated crater repairs. Descriptions of the geocell products and their properties determined through laboratory testing were provided in Chapter 3.

4.1 Soils

Each soil was classified according to the Unified Soil Classification System (ASTM 2017a). Specific gravity (ASTM 2014c) was determined, and modified proctor testing (ASTM 2012) and laboratory California bearing ratio (CBR) testing (ASTM 2016a) were performed on each soil. A summary of the soil properties is shown in Table 4.1. The compaction curves and laboratory CBR testing results are shown in Figure 4-1 and Figure 4-2, respectively. The grain-size distribution curves for the soils are provided in Appendix B.

Table 4-1. Soil characteristics and classification data.

Soil type	Poorly Graded Sand (SP)	Low Plasticity Clay (CL)	Poorly Graded Gravel with Silt and Sand (GP-GM)	Clayey Sand with gravel (SC)	Well-Graded Gravel with Sand (GW)	Silty Clay (CL-ML)	Clayey Sand (SC)
Specific gravity	2.65	2.75	2.73 (*est.*)	2.69	2.67	2.79 (*est.*)	2.68 (*est.*)
Optimum water content (%)	1.9	14.5	5.1	5.5	0.4	12.7	8.1
Maximum dry density (pcf)	111.5	115.0	147.4	137.5	119.8	117.4	130
CBR at optimum water content (%)	20.5 (*est.*)	57 (*est.*)	100	37.2	25	65	29.1
Cc	0.85	–	3.86	2.61	2.21	–	7.17
Cu	2.27	–	59.31	22.78	8.56	–	17.04
LL	–	37	–	34	–	23	34
PI	–	14	–	21	–	7	13
Finer than #200	1.7	100	8.8	17.5	3	100	13.9

Notes: Cc = coefficient of curvature, Cu = uniformity coefficient, LL = liquid limit, PI = plasticity index, *est.* = estimated

Figure 4-1. Compaction curves for the soils.

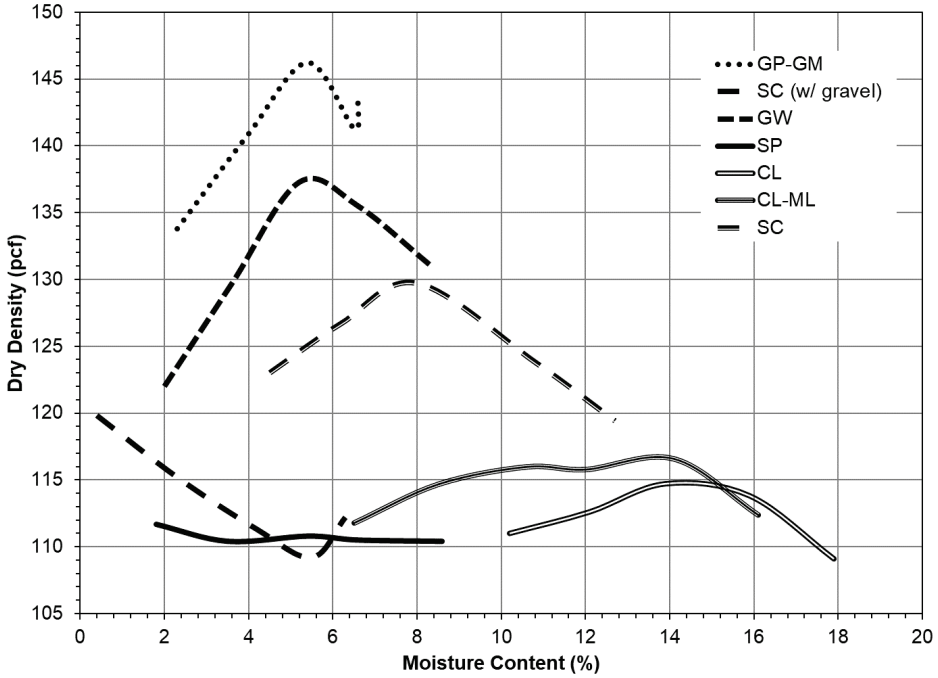

Figure 4-2. Laboratory CBR data for the soils.

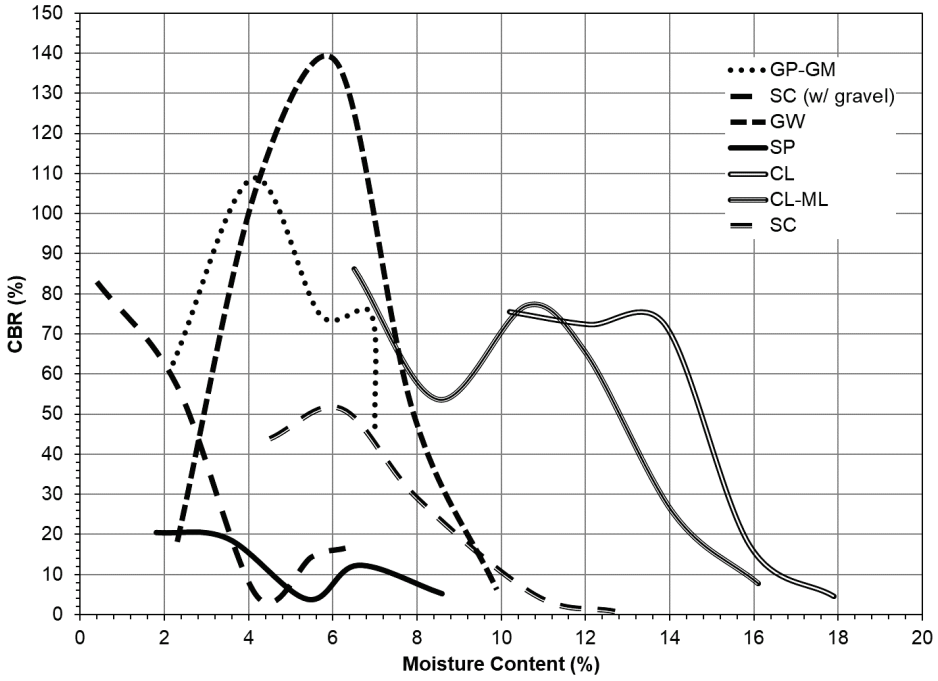

To evaluate the influence of geocells, most field experiments were carried out using a concrete sand as filling material. The material was purchased from a local gravel pit and was classified as a poorly graded sand (SP).

The geocell-reinforced backfill was placed over a low-plasticity clay (CL) subgrade to provide a uniform foundation throughout the tests. The material was purchased from a locally available borrow pit and was classified as a low-plasticity clay (CL).

Crushed limestone was used as the capping material in Phase 1 and as a geocell-reinforced backfill material in Phase 4. The material was classified as a poorly graded gravel with silt and sand (GP-GM).

In addition to GP-GM and SP, Phase 4 included four more backfill materials that were reinforced with geocells. These were the following:

- A blend of clay and gravel that resulted in 33.8% gravel, 48.7% sand, and 17.5% clay. The material was classified as a clayey sand with gravel (SC). From herein, this material will be referred to as "SC with gravel."
- A blend of clay and sand that resulted in 6.5% gravel, 79.6% sand, and 13.9% clay. The material was classified as a clayey sand (SC).
- A crushed river gravel. This material was meant to represent a medium-quality material, since not all faces of the gravel aggregate were fractured faces and were, therefore, rounded. The material was purchased from a local source and was classified as a well-graded gravel with sand (GW).
- Silty clay (CL-ML) was also used to represent a low-quality material. It was purchased from a local borrow pit.

4.2 Geotextile

A 6-oz. nonwoven, needle-punched, polypropylene geotextile fabric was used at the interface of geocell layers and at the surface of the CL subgrade layer. It was purchased from US Fabrics Inc. and delivered in a roll that was 12 ft wide and 360 ft long (product US 160NW.)

4.3 Construction tools and equipment

Equipment used for the initial steps in the repair process--cutting, breaking, and excavating--were the following: (1) a 60-in. wheel saw attachment (Caterpillar SW60) on a Caterpillar compact track loader (CTL 279C), (2) a moil-tipped hydraulic breaker (Bobcat HB1180) on a mini-excavator (Bobcat E45 T4), and (3) a bucket attachment on a mini-excavator.

Equipment that was used throughout the construction of the backfill were material handling equipment, such as a CTL 279C with bucket attachment and a front-end loader. These were used to transport backfill materials and the geotextile and geocell sections to the repairs. Cutting tools that were used for preparing the geotextile and geocell sections included utility knives, a reciprocating saw, a measuring tape, and rebar. Hammers, backfill rakes, and shovels were also in the tool set to assist with preparation of the backfill in the repair. A 10-kip capacity telehandler was used to transport the FRP FOD cover panels, as well as the packaged kit with installation tools and equipment.

To compact the SP, a JPC-80 vibratory plate compactor was used. The walk-behind plate compactor weighed 190 lb and produced a centrifugal force of 3,968 lb. The plate size was 1.77 ft by 1.38 ft. A Multiquip Mikasa MTX-70 rammer was used for compacting the CL subgrade and the GP-GM, SC with gravel, GW, SC, and CL-ML backfill materials. The rammer had an operating weight of 165 lb and an impact force of 2,855 lb. On the surface of the repairs, a CV18B vibratory drum compactor was attached to a CAT 279C High Flow CTL (skid steer). Photographs of each compaction device are shown in Figure 4-3.

Figure 4-3. Photographs of compaction equipment.

JPC-80 vibratory plate compactor.

Multiquip Mikasa MTX-70 rammer.

CAT CV18B vibratory drum compactor attachment.

4.4 Fiberglass-Reinforced Polymer (FRP) FOD cover system

The FRP FOD cover panels were made of layers of glass fiber and aramid fabric impregnated with polyester resin (Rushing et al. 2016). A full panel measured 18 ft by 6.6 ft, and a half-panel measured 9.3 ft by 6.6 ft. Each panel was connected using metal bushings and bolts. One repair required one full panel and two half-panels. The leading and trailing edges of the panel were anchored to the pavement by using a heavy-duty sleeve concrete expansion anchor (Power Bolt 6957.) Twenty anchors were required for each panel, based on the number of holes available in the leading and trailing edges of the repair. The leading edge had a full anchor panel attached. Photographs of the FRP FOD cover panel system are shown in Figure 4-4.

Figure 4-4. FRP FOD cover system.

FRP panels assembled.

Connector bushings.

Anchor bushing and concrete expansion anchor.

5 Full-Scale Testing

5.1 Preparation of simulated craters

Each simulated crater was initially prepared by cutting the portland cement concrete (PCC) surface with a CAT SW60 wheel saw powered by a CAT CTL 279C, which was representative of cutting around upheaval in a realistic scenario. Once the repair was cut to size, the PCC was broken into smaller pieces with a moil-tipped hydraulic breaker attachment (Bobcat HB1180) on a mini-excavator (Bobcat E45 T4.) Large debris and material underneath the PCC surface were then removed with a bucket attachment on a mini-excavator. Each crater was excavated to a minimum depth of 34 in. A CL foundation was placed to ensure similar foundation conditions for each evaluation. The CL layer was placed in approximately 3- to 4-in.-thick compacted lifts (5- to 6-in.-thick loose lifts.) Compaction of each lift was completed by applying two coverages with a Multiquip Mikasa MTX70 HD Rammer. A coverage consisted of starting compaction in one corner of the repair and working towards the center of the repair in a circular motion, and then returning in a circular motion towards the corner where compaction began. Photographs of crater preparation are show in Figure 5-1.

Figure 5-1. Preparation of simulated crater.

(a) Cutting with SW60 attachment.

(b) Breaking with moil-tipped hammer attachment on the mini-excavator.

(c) Compaction of the CL layer with the rammer.

5.2 Preparation of geotextile and geocell materials

Once the surface of the CL layer was finished, the horizontal dimensions of the crater were measured (8.5 ft x 8.5 ft) so that the geocell sections and geotextile could be cut to size. The geotextile was cut using a utility knife.

Different methods could be used to determine the number of geocell sections that are required and the number of cells each section needs to have in length and width. In cases where the repair length is different from the repair width, the sections for the first layer of the geocell-reinforced backfill may not be the same size as the sections for the second layer, since the top layer is placed transverse to the bottom layer.

The simplest method was to drive a piece of rebar (or similar tool) in the ground in a square of the same dimensions as the repair. Each of the rebar stakes represented the corners of the repair. An additional rebar was placed between these to prevent the geocell section from collapsing.

To cut the first layer of geocells, the corners of a geocell section were placed at two of the corner stakes and then expanded in what represented the direction of traffic (since the first geocell layer is expanded parallel to the direction of traffic.) The section was fully expanded until the individual cell length was the length shown in Table 3-1. For example, the individual cell length for EGA208PT when fully expanded was required to be around 8.8 in. This was important because, in order for the geocell-reinforced backfill to perform correctly, the cells needed to be fully expanded when filled. Smaller or collapsed cells may not provide adequate reinforcement. While fully expanded, the excess length of the geocell section was trimmed using a utility knife. Each cell was cut individually and carefully so as not to cut excess material.

The Geoweb, Neoweb, and EnviroGrid products had an expanded section width of 8 ft to 9 ft. The full width of these sections was used for the repairs and did not require excess material to be removed. The Typar 220/200 product, however, had to be cut in width since the expanded section width was 20 ft. To cut the excess width, the section was removed from the rebar and allowed to collapse. The reciprocating saw was used to cut at the next weld.

The second layer of geocells was cut in the manner described above. The most important difference was that the sections were expanded in what

represented the direction perpendicular, or transverse, from the direction of traffic. Since the repairs had the same length and width, i.e., 8.5 ft x 8.5 ft, the section sizes were the same as the sections for the first layer. Photographs of the cutting process are shown in Figure 5-2. Note that Phase 5 repairs required additional sections of geotextile and geocells. These were cut in the same manner.

Figure 5-2. Cutting geotextile and geocell.

(a) Cutting geotextile.

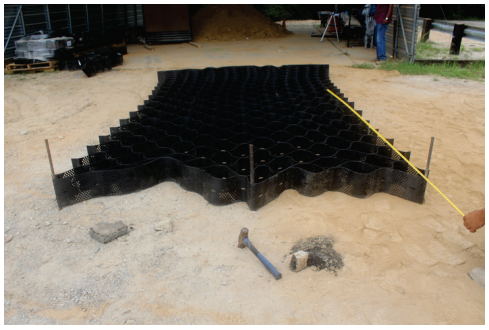

(b) Geocell section placed on rebar for cutting.

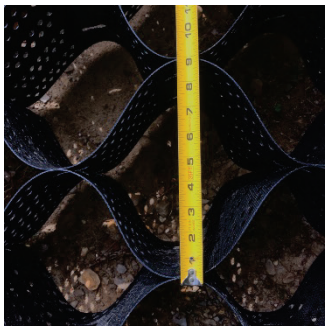

(c) Checking individual cell length.

(d) Cutting the length of the geocell section.

(e) Utility knife used to cut geocell section length.

(f) Reciprocating saw used to cut geocell section width.

5.3 Construction of geocell-reinforced backfill

The installation of the geocell-reinforced backfill for each repair is discussed in the following paragraphs. The procedure provided in UFC 3-270-07 (Department of Defense 2002) was applied throughout the construction process. Schematics of the direction of expansion for the first and second layers of geocells are shown in Figure 5-3 and Figure 5-4.

1. The surface of the CL layer was lined with a non-woven geotextile (Figure 5-5a).
2. Rebar was placed at all corners of the repair. The first layer of geocells was expanded parallel to the centerline (direction of traffic) (Figure 5-3). The corners of the geocell were placed at the rebar to hold the expanded geocell section in place. Soil was used to fill some of the geocell pockets along the edges to help hold the section in place (Figure 5-5b).

Figure 5-3. Direction of expansion of first geocell layer.

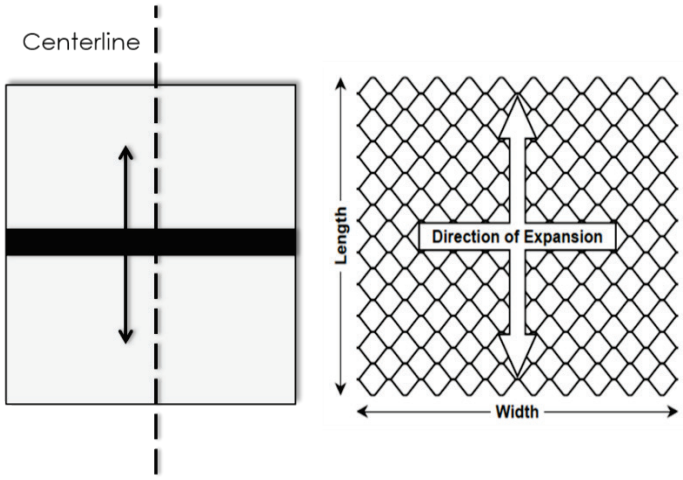

3. The geocell section was backfilled by dropping the soil vertically into the repair to avoid displacing the section (Figure 5-5c). The section was overfilled by approximately 2 in., and the soil was spread evenly (Figure 5-5d).
4. The soil was compacted using a plate compactor (Figure 5-5e) or rammer (Figure 5-5f). Any excess material was struck level with the top of the geocells.

The number of coverages applied for each material was the following: two coverages using the plate compactor for SP; three coverages for GP-GM

using the rammer; three coverages for SC with gravel using the rammer; four coverages for GW using the rammer; four coverages for the SC using the rammer; four coverages for the CL-ML using the rammer.

5. The surface of the first layer of geocells was lined with the geotextile.
6. Rebar was placed at all corners of the repair. The second layer of geocells was expanded perpendicular to the centerline (across from the direction of traffic; Figure 5-4). The corners were placed at the rebar to hold the expanded geocell section in place. Soil was used to fill some of the geocell pockets along the edges to help hold the section in place.

Figure 5-4. Direction of expansion of second geocell layer.

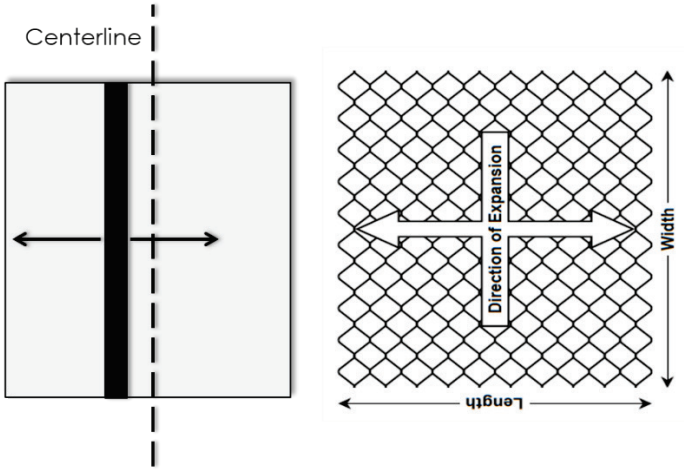

7. The second layer of geocells was backfilled by dropping the soil vertically into the repair to avoid displacing the section. The section was overfilled by approximately 2 in., and the soil was spread evenly. The soil was compacted using a plate compactor or rammer.
8. For Phase 5 repairs, the next layer(s) was (were) built using the same process.
9. The top layer of geocell-reinforced backfill was compacted with the CV18B vibratory drum compactor attachment, as shown in Figure 5-5g and Figure 5-5h (Phases 2 to 5). Compaction with the CV18B attachment was carried out as shown in Figure 5-6. A 1- to 2-in. (max) buffer of backfill material was left above the top reinforced layer prior to installing the FRP FOD cover to avoid direct contact between the geocells and the FOD cover.

UFC 3-270-07 (Department of Defense 2002) recommends at least two (2) passes with a vibratory roller, but smaller compaction equipment was used

for the repairs in this report. Therefore, the minimum number of coverages was determined once the dry density was at least 90% of the maximum dry density (measured with the nuclear gage.) A coverage consisted of starting compaction in one corner of the repair, working towards the center of the repair in a circular motion, and then returning in a circular motion towards the corner where compaction began.

Figure 5-5. Geocell-reinforced backfill construction process.

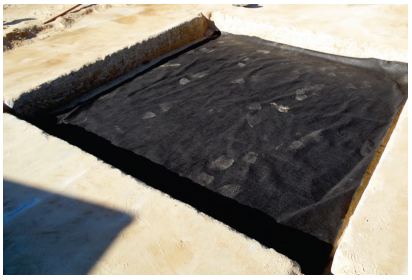

(a) Geotextile placed on subgrade.

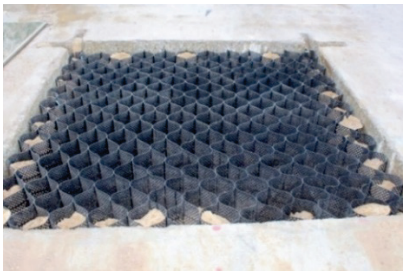

(b) Geocell section secured at edges with SP.

(c) Backfilling with SP.

(d) Spreading GW evenly over geocell section.

(e) Compacting SP with plate compactor.

(f) Compacting SC with rammer.

(g) Compacting SP with CV18B attachment.

(h) Compacting GP-GM with CV18B attachment.

Figure 5-6. Compaction coverage with the CV18B attachment on the CTL.

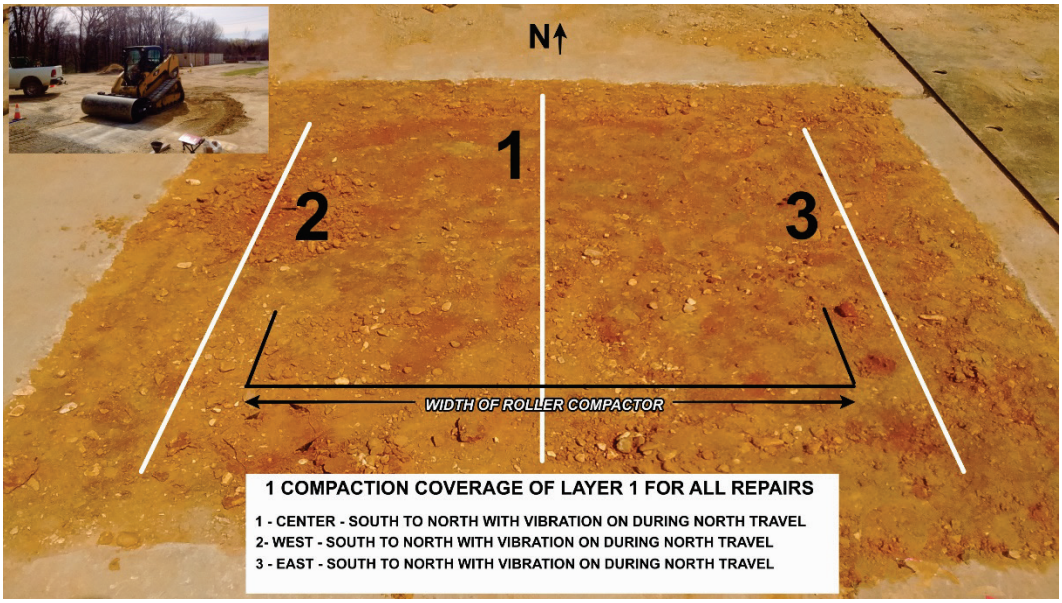

Figure 5-7 shows photos of the different backfill materials reinforced with geocells. The SP backfill in the control repairs that did not have geocell reinforcement was built in 6-in.-thick compacted lifts. Each lift was compacted using a plate compactor. In Phase 1, the 4-in. GP-GM cap was compacted with a CV18B vibratory roller attachment on a CTL.

Figure 5-7. Different backfill soils reinforced with geocells.

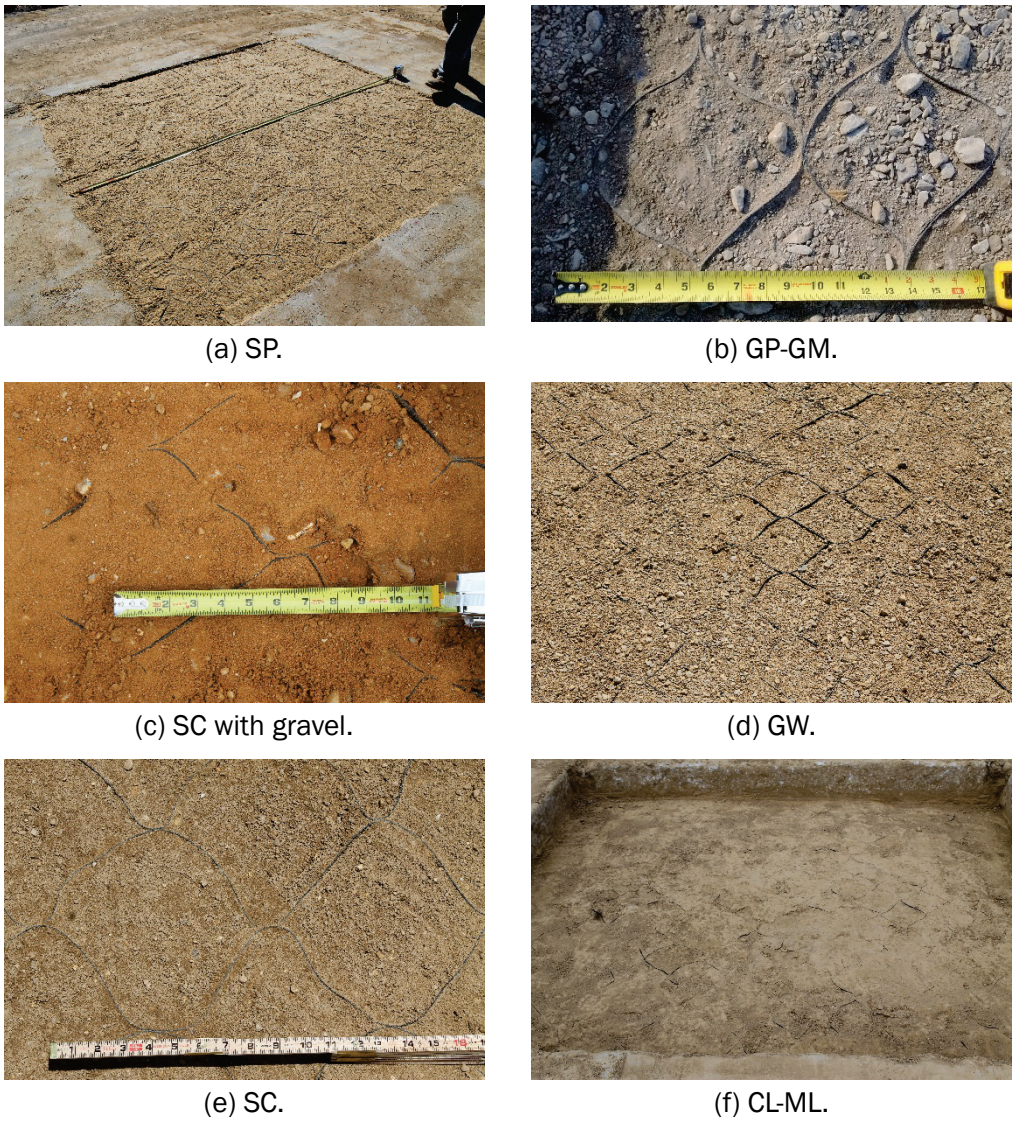

(a) SP. (b) GP-GM.

(c) SC with gravel. (d) GW.

(e) SC. (f) CL-ML.

5.4 Repair capping

The capping material used in Phase 1 was 4 in. (compacted) of GP-GM. The material was placed in one lift with a bucket attachment on a CTL and hand-raked until it was approximately 1 in. to 2 in. above the original PCC surface. Around 2 gal of water was added to assist with compaction. Two coverages were applied with a rammer and then compacted with a CV18B vibratory roller attachment (as defined in Figure 5-6). Photographs of capping material construction are shown in Figure 5-8.

Figure 5-8. Construction of GP-GM repair cap.

Placing GP-GM in repair.

Raking GP-GM.

Compacting GP-GM with CV18B.

The FRP FOD cover was used as the capping method in Phase 2 through Phase 5. A layout of the panels is shown in Figure 5-9. This assembly can be used for repairs up to 10 ft in diameter (Rushing et al. 2016). Photographs showing the installation of the FRP FOD cover are shown in Figure 5-10. Rushing et al. (2016) provides details on the procedures, tools, and equipment required for installation of the FRP FOD cover and placement of the Power Bolt 6957 concrete anchor bolts.

Figure 5-9. FRP FOD cover layout.

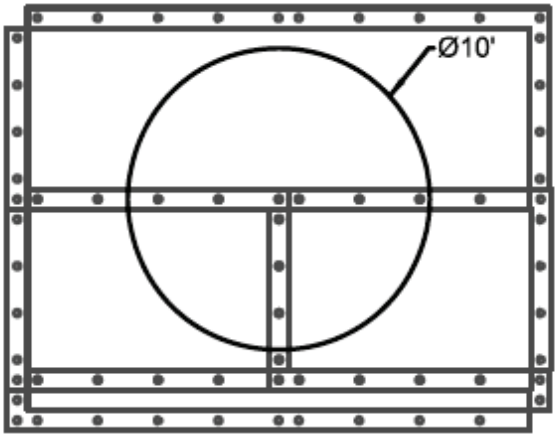

Figure 5-10. Installation of FRP FOD cover.

(a) Assembled panels.

(b) Applying torque to connector bushing bolt.

(c) Drilling through PCC.

(d) Placing concrete anchor.

(e) Applying torque to concrete anchor bolt.

5.5 Construction data collection and results

Quality control tests performed during construction are listed in Table 5-1. A sand cone test was performed on each layer of the geocell-reinforced backfill to determine the wet and dry density. The test was performed at one location on each layer within a single cell of the geocell-reinforced backfill (Figure 5-11a). Nuclear moisture data, nuclear wet density data, and oven dry moisture data were collected on the CL layer, on each lift of the geocell-reinforced backfill, and on the surface of the GP-GM cap. The direct

transmission method of the nuclear gauge was used for field-testing at three locations per layer. For the geocell-reinforced backfill, the rod was inserted at the center of a single cell (Figure 5-11b). Oven moisture samples were obtained from the same locations where nuclear moisture data were collected. Dynamic Cone Penetrometer (DCP) testing was performed on the surface of the CL, the backfill, and on the surface of the GP-GM cap in Phase 1 to approximate an in-place CBR; Figure 5-11c). Rod and level measurements were taken during construction to verify layer thicknesses. After trafficking was completed, posttest forensics included nuclear moisture and density data collection, DCP data collection, and rod and level measurements. The latter were collected to measure the rut depth at different depths.

Table 5-1. In-situ data collection during construction.

Test Name	Standard
Standard Test Methods for In-Place Density and Water Content of Soil and Soil-Aggregate by Nuclear Methods (Shallow Depth)	ASTM D 6938 (2017b)
Standard Test Method for Density and Unit Weight of Soil in Place by the Sand Cone Method	ASTM D 1556 (2015)
Standard Test Method for Laboratory Determination of Water Content of Soil and Rock Mass	ASTM D 2216 (2019)
Standard Test Method for Use of the Dynamic Cone Penetrometer in Shallow Pavement Applications	ASTM D 6951 (2018)
Standard Test Method for Nonrepetitive Static Plate Load Tests of Soils and Flexible Pavement Components, for Use In Evaluation and Design of Airport and Highway Pavements	ASTM D1196 (2016b) / CRD-C 655-95 (1995)

Figure 5-11. In-situ soil testing.

(a) Sand cone test.

(b) Nuclear moisture and density gauge test.

(c) DCP test.

Most of the data collection discussed was focused on characterizing the soil properties with and without reinforcement. However, the DCP is not a clear indicator of improvement in bearing capacity due to geocell reinforcement. Therefore, static plate load tests were performed on each layer of the repairs in Phase 1 to determine the modulus of subgrade reaction (k). Since the test is time-consuming, it was performed only in Phase 1 to demonstrate the improvement in k value with geocell reinforcement.

A tractor and trailer with an anchored frame were loaded to provide 25,000 lb of reaction weight and were used in conjunction with a hydraulic jack capable of applying a 25,000 lb total load. To conduct the test, 1-in.-thick nested steel bearing plates--18, 24, and 30 in. in diameter--were placed on the soil layer with a thin layer of clean sand (less than 1 in.) to assist in providing a level surface. Three dial micrometers were used to measure the displacement during loading. Custom software written by ERDC was used to monitor the testing process and estimate the k value. The tests were conducted according to ASTM D1196 (2016b), and CRD-C 655-95 (1995) was consulted for detailed test instructions. Photographs of the static plate load test on the CL layer are shown in Figure 5-12.

Figure 5-12 Plate bearing test.

(a) Overall view of plate bearing test.

(b) Closeup view of plate bearing test.

The in-situ soil properties of all repairs are reported in Table 5-2 through Table 5-6. Any data that showed discrepancies and clearly showed outliers were not reported. Note that there were some clear differences between the nuclear gauge density and the sand cone density measured in repairs that were reinforced with geocell in the backfill layer. It is possible that the nuclear gauge readings were affected by the geocell materials. The CBR determined from the DCP at the top of the SP was not reported due to lack of confinement of the SP at the top 6 in. to 8 in. The following paragraphs discuss the construction data in each phase individually.

In Phase 1, the reported CBRs were from DCP data collected on the day that trafficking was started. For the GP-GM cap, this represents up to 7 days of curing time in each repair, since the cap was placed and compacted on different dates during a period of one workweek. The CBR data on the CL layer were very low (less than 2 CBR) on the day trafficking started. This was due to the occurrence of a rain event that allowed groundwater to penetrate into the CL layer. Since all the construction was completed and trafficking was scheduled to start, the traffic tests were performed, keeping in mind that the number of pass levels sustained would likely be lower than expected. The nuclear density and moisture data on the CL layer, however, were from the date of construction of that layer. According to the data collected with the sand cone, the dry density of the SP in the geocell-reinforced repairs was more than the maximum dry density achieved in the laboratory, while the SP in the Control repair had a density greater than 95% maximum dry density.

Table 5-2. In-situ soil properties for Phase 1 repairs.

		No Geocell	Individual Cell Length x Width (in.)		
		C-1	1-A	1-B	1-C
Layer	Property	Control	8.8 x 10.2	11.3 x 12.6	18.7 x 20
GP-GM	Nuclear WD (pcf)	138.2	146.5	149.4	144.8
	Nuclear DD (pcf)	133.8	142.5	144.2	138.6
	Nuclear MC (%)	4.4	4	5.2	6.275
	CBR	50	100	70	100
	k (psi/in.)	163	118	108	126
	Thickness (in.)	4.67	5.4	4.8	4.6
Geocell-Reinforced SP (Layer 2)	Nuclear WD (pcf)	113.2	110.6	109.9	113.3
	Nuclear DD (pcf)	108.7	104.9	105.6	107.7
	Nuclear MC (%)	3.57	5.42	4.07	5.17
	Oven MC (%)	4.7	5.3	4.1	6.2
	Sand Cone WD (pcf)	115.2	124.3	120.9	122.5
	Sand Cone DD (pcf)	110.2	117.7	116.6	115.7
	Sand Cone Oven MC (%)	4.53	5.59	3.72	5.86
	CBR	9	15	14	14
	k (psi/in.)	116	59	49	108
	Thickness (in.) [Layer 1 and 2]	15.9	15.1	15.4	15.3
Geocell-Reinforced SP (Layer 1)	Nuclear WD (pcf)	111.4	108.5	110.5	113.8
	Nuclear DD (pcf)	106.4	102.8	106.5	109.0
	Nuclear MC (%)	4.67	5.50	3.76	4.43
	Oven MC (%)	5.0	4.5	3.7	4.7
	Sand Cone WD (pcf)	117.0	118.2	123.6	120.5
	Sand Cone DD (pcf)	111.7	112.5	119.9	115.6
	Sand Cone Oven MC (%)	4.82	5.03	3.1	4.25
	CBR	6	12	12	13
CL	Nuclear WD (pcf)	99.7	103.3	111.1	107.0
	Nuclear DD (pcf)	87.6	91.9	99.4	94.5
	Nuclear MC (%)	13.2	12.5	11.75	13.8
	Oven MC (%)	-	12.6	14.8	13.8
	CBR	0.2	1.3	1	1.5
	k (psi/in.)	45	84 / 119	81	83
	Thickness (in.)	14	14.1	14.2	13.8

WD= Wet Density; DD = Dry Density; MC=Moisture Content; CBR = California bearing ratio

In Phase 2, the CBRs reported were also from DCP data collected on the first day that trafficking was started. In general, it was noted that the dry density of the geocell-reinforced SP was higher for thinner layers (e.g., 117.9 pcf for a 4-in. layer vs 114.2 pcf for an 8-in. layer.) This indicated better compaction was generally achieved when using a shorter geocell height. The oven moisture of the SP was lower than in Phase 1. According

to the data collected with the sand cone, the dry density of the SP was more than the maximum dry density achieved in the laboratory.

Table 5-3. In-situ soil properties for Phase 2 repairs.

		No Geocell	Thickness of Reinforcement		
		C-2	2-C	2-B	2-A
Layer	Property	Control	2 layers of 4–in. geocell (8 in.)	2 layers of 6-in. geocell (12 in.)	2 layers of 8-in. geocell (16 in.)
Geocell-Reinforced SP (Layer 2)	Nuclear WD (pcf)	113.7	114.6	110.3	109.6
	Nuclear DD (pcf)	110.7	109.7	107.4	106.4
	Nuclear MC (%)	2.7	4.5	2.8	2.9
	Oven MC (%)	3.1	3.7	2.9	3.1
	Sand Cone WD (pcf)	—	124.2	119.6	117.7
	Sand Cone DD (pcf)	—	117.9	116.3	114.2
	Sand Cone Oven MC (%)	—	5.4	2.9	3.1
	Thickness (in.)	7.4	4.5	6.9	9.2
Geocell-Reinforced SP (Layer 1)	Nuclear WD (pcf)	112.7	110.8	110.0	107.8
	Nuclear DD (pcf)	109.6	106.4	107.0	104.6
	Nuclear MC (%)	2.8	4.2	3.3	3.0
	Oven MC (%)	3.0	3.2	2.1	2.3
	Sand Cone WD (pcf)	—	120.0	119.2	115.0
	Sand Cone DD (pcf)	—	116.5	116.7	112.5
	Sand Cone Oven MC (%)	—	2.7	2.1	2.3
	CBR	7.0	4.5	5.0	4.0
	Thickness (in.)	9.4	4.0	6.0	8.0
CL	Nuclear WD (pcf)	112.0	102.9	106.4	107.0
	Nuclear DD (pcf)	99.9	91.8	97.1	94.8
	Nuclear MC (%)	12.3	12.1	9.6	12.8
	Oven MC (%)	16.1	15.6	11.6	15.9
	CBR	8.0	8.0	8.0	9.0
	Thickness (in.)	16.8	25.5	20.6	16.2

Note: CBR determined from the DCP at the top layer was not reported due to lack of confinement of the SP at the top 6 in. to 8 in.

WD= Wet Density; DD = Dry Density; MC=Moisture Content

The CBRs reported for Phase 3 were also from DCP data collected on the first day that trafficking was started. Repairs 3-A and 3-B were built first, followed by Repairs 3-C and 3-D.

Table 5-4. In-situ soil properties for Phase 3 repairs.

Layer	Property	Geocell Product			
		3-A	3-B	3-C	3-D
		Neoweb	EnviroGrid	Geoweb	GeoCell GS
Geocell-Reinforced SP (Layer 2)	Nuclear WD (pcf)	112.1	111.3	110.9	110.3
	Nuclear DD (pcf)	107.2	106.3	105.8	106.2
	Nuclear MC (%)	4.6	4.7	4.8	3.9
	Oven MC (%)	3.5	4.1	4.0	—
	Sand Cone WD (pcf)	121.0	118.8	113.2	112.7
	Sand Cone DD (pcf)	117.5	115.1	109.2	108.6
	Sand Cone Oven MC (%)	3.0	3.3	3.7	3.8
	Thickness (in.)	9.4	9	9.4	8.9
Geocell-Reinforced SP (Layer 1)	Nuclear WD (pcf)	109.6	108.8	114.1	115.5
	Nuclear DD (pcf)	105.4	105.0	112.0	111.8
	Nuclear MC (%)	3.9	3.7	4.1	3.4
	Oven MC (%)	4.5	3.5	4.2	4.6
	Sand Cone WD (pcf)	119.6	–	117.5	—
	Sand Cone DD (pcf)	115.9	–	112.5	—
	Sand Cone Oven MC (%)	3.3	–	4.4	—
	CBR	5	4	5	4
	Thickness (in.)	7.9	8	8	8
CL	Nuclear WD (pcf)	111.7	107.5	100.0	111.2
	Nuclear DD (pcf)	99.3	95.4	88.9	100.9
	Nuclear MC (%)	12.4	12.8	12.5	10.2
	Oven MC (%)	13.5	14.0	14.4	12.2
	CBR	8	8	8	8
	Thickness (in.)	17.8	17.0	16.4	17.6

Note: CBR determined from the DCP at the top layer was not reported due to lack of confinement of the SP at the top 6 in. to 8 in.

WD= Wet Density; DD = Dry Density; MC=Moisture Content

Phase 4 was separated into two parts to assist with construction and with the number of craters available for performing the test. Repairs 4-A, 4-B, and 4-C were built and trafficked to completion first, followed by Repairs 4-D, 4-E, and 4-F. The CBRs reported were from data collected on the first day of trafficking. The top layers of 4-A and 4-B were placed 12 days before the start of traffic. This time was needed to finish the construction in Repair 4-C and to allow the materials to cure properly. However, the GP-GM in 4-A was able to achieve a pretest value of only 30 – 35 CBR. Most materials had a dry density higher than the maximum dry density measured in the laboratory (according to sand cone test data.) The GP-GM and the CL-ML had densities that were at least 90% of maximum dry density.

Table 5-5. In-situ soil properties for Phase 4 repairs.

Layer	Property	Backfill Soil					
		4-A	4-B	4-C	4-D	4-E	4-F
		GP-GM	SC w/ gravel	SP	GW	SC	CL-ML
Geocell-Reinforced Soil (Layer 2)	Nuclear WD (pcf)	141.9	121.0	112.7	116.4	132.1	115.7
	Nuclear DD (pcf)	135.7	114.9	108.5	112.5	120.8	98.8
	Nuclear MC (%)	4.6	5.3	3.7	3.5	9.4	17.4
	Oven MC (%)	4.0	3.3	—	2.0	6.9	15.3
	Sand Cone WD (pcf)	141.6	144.8	126.8	138.7	141.9	125.8
	Sand Cone DD (pcf)	136.9	135.8	121.0	136.6	128.3	106.2
	Sand Cone Oven MC (%)	3.4	6.7	4.8	1.6	10.6	18.5
	CBR	30	23	—	20	19	11
	Thickness (in.)	9.4	9.6	9.8	9	9.8	9.6
Geocell-Reinforced Soil (Layer 1)	Nuclear WD (pcf)	150.8	127.6	112.6	113.4	128.1	116.3
	Nuclear DD (pcf)	142.6	123.8	108.6	108.7	118.6	100.3
	Nuclear MC (%)	5.7	6.3	3.7	4.3	7.7	16.1
	Oven MC (%)	3.1	7.3	3.4	2.7	7.0	15.1
	Sand Cone WD (pcf)	—	—	118.3	136.7	142.6	129.7
	Sand Cone DD (pcf)	—	—	115.8	133.4	132.8	111.8
	Sand Cone Oven MC (%)	—	—	2.2	2.4	7.4	16.1
	CBR	35	20	9	30	25	11
	Thickness (in.)	7.9	7.9	7.8	8	7.8	7.8
CL	Nuclear WD (pcf)	118.4	122.5	116.9	114.1	114.0	114.3
	Nuclear DD (pcf)	102.4	106.4	102.2	99.9	99.4	100.3
	Nuclear MC (%)	15.7	15.1	14.6	14.4	14.7	13.9
	Oven MC (%)	17.2	16.6	16.1	16.3	16.3	15.7
	CBR	9	8	11	17	17	17
	Thickness (in.)	17	16.8	16.4	16.4	16.3	16.9

*Note: CBR determined from the DCP at the top layer was not reported for SP due to lack of confinement of the SP at the top 6 in. to 8 in.

WD= Wet Density; DD = Dry Density; MC=Moisture Content

Phase 5 repairs were built and tested a few months after the completion of Phase 4. The CBR data reported were from the day before trafficking began. Sand cone tests were not performed due to time constraints, since Phase 5 was performed as additional verification to the results obtained in Phase 2 (i.e., down-selection of geocell height.) In general, the dry density of the 6-in.-thick layers was higher than that of the 8-in.-thick layers.

Table 5-6. In-situ soil properties for Phase 5 repairs.

Layer	Property	Layers of Reinforcement	
		5-A	5-B
		Four 6-in. geocell layers	Three 8-in. geocell layers
Geocell-Reinforced SP (Layer 4)	Nuclear WD (pcf)	108.8	—
	Nuclear DD (pcf)	103.7	—
	Nuclear MC (%)	5.0	—
	Oven MC (%)	3.8	—
	Thickness (in.)	7.9	—
Geocell-Reinforced SP (Layer 3)	Nuclear WD (pcf)	110.6	109.1
	Nuclear DD (pcf)	103.5	103.8
	Nuclear MC (%)	6.8	5.1
	Oven MC (%)	6.6	4.6
	CBR	5.6	—
	Thickness (in.)	5.8	9.9
Geocell-Reinforced SP (Layer 2)	Nuclear WD (pcf)	110.1	105.3
	Nuclear DD (pcf)	103.1	99.9
	Nuclear MC (%)	6.7	5.5
	Oven MC (%)	6.5	4.9
	CBR	9.0	6.7
	Thickness (in.)	6.1	8.0
Geocell-Reinforced SP (Layer 1)	Nuclear WD (pcf)	108.0	105.0
	Nuclear DD (pcf)	101.6	100.4
	Nuclear MC (%)	6.7	4.6
	Oven MC (%)	6.6	4.5
	CBR	9.6	8.3
	Thickness (in.)	5.8	7.9
CL	Nuclear WD (pcf)	118.6	117.2
	Nuclear DD (pcf)	104.2	103.6
	Nuclear MC (%)	13.8	13.1
	Oven MC (%)	15.7	17.0
	CBR	17.0	15.0
	Thickness (in.)	8.8	8.8

Note: CBR determined from the DCP at the top layer was not reported due to lack of confinement of the SP at the top 6 in. to 8 in.

WD= Wet Density; DD = Dry Density; MC=Moisture Content

5.6 Trafficking and data collection

Simulated aircraft traffic was applied to the repairs with a single-wheel C-17 load cart equipped with a 50-in. by 21-in. 30-ply tire inflated to 142 psi and loaded so that the test gear was supporting 38,500 lb (Figure 5-13). This configuration represented the maximum load on one tire of a C-17 aircraft

allowed in contingency operations. A normally distributed traffic pattern with a total wander with of 4.5 ft was used to apply test traffic to each repair. Traffic was applied by driving the load cart forward and then backward in the same wheel path then moving laterally approximately one tire width on each forward pass. Tire position was maneuvered outside the traffic area.

Figure 5-13. Trafficking with the single-wheel C-17 load cart on the finished repairs.

(a) Single-wheel C-17 load cart.

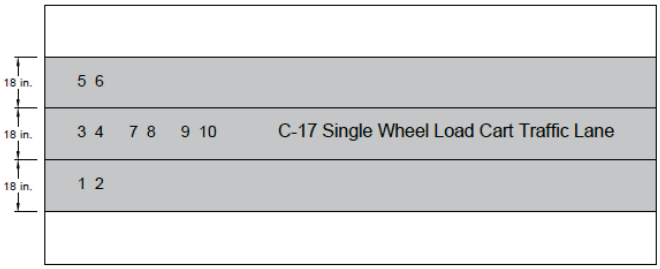

(b) Traffic pattern.

Data collection efforts included rod and level measurements at 1-ft intervals along the centerline and at two cross sections that were offset 3 ft from the edges of the repair (Figure 5-14a). Rod and level measurements along the cross section were taken on the GP-GM cap or on the loaded FRP FOD cover surface, where two (2) 1-kip blocks (much less weight than the load cart) were placed next to the cross section (Figure 15-14b). This was an attempt to measure the permanent deformation of the backfill throughout trafficking without having to disassemble the panels, since the FRP FOD cover tended to bridge over any deformation on the underlying reinforced backfill. All measurements were taken prior to trafficking, at select pass levels throughout trafficking, and after completion of trafficking. The results reported in Chapter 6 included upheaval measured on each side of the rut. Measurements were also taken during construction and after completion of trafficking at each construction layer to measure the deformation at different depths.

Figure 5-14. Data collection on the surface of the FRP FOD cover.

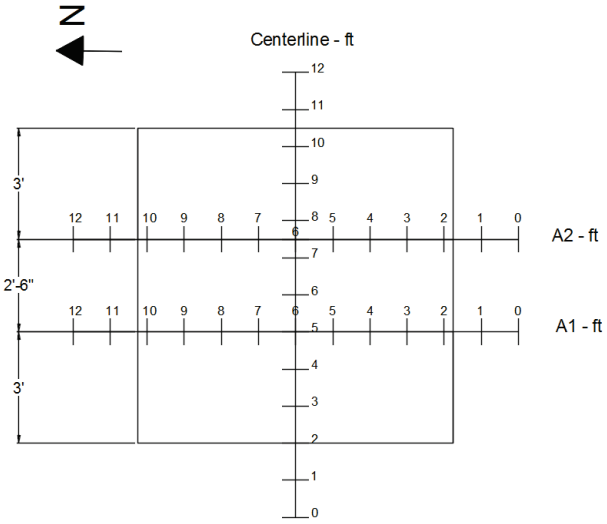

(a) Data collection locations on the GP-GM and FRP FOD caps.

(b) Loaded cross-section measurements on the FRP FOD cover.

5.7 Failure criteria

UFC 3-270-07 (Department of Defense 2002) defines expedient repairs as airfield pavement repairs executed in the most expeditious manner possible that create an initial operationally capable minimum operating strip and sustains 100 C-17 passes or 100 C-130 passes. The failure criterion established was the development of 3 in. of permanent surface deformation for C-17 traffic. Deformation measured in this test program includes any upheaval that developed outside the traffic lanes.This failure criterion was developed based upon USAF requirements (USAF 1992). Therefore, the repair was required to sustain 100 passes of the C-17 load cart before 3 in. of deformation occurred to be deemed successful.

6 Results and Discussion

6.1 Phase 1 repairs

Phase 1 repairs failed quickly after trafficking began. The load cart tire sheared through the surface of the repairs and created a large hole where the tire punched through (Figure 6-1). The first repair to fail was the Control repair, followed by Repair 1-C, then 1-B, and then 1-A. The final pass number on Repair 1-A was 13 passes. Repairs 1-B, 1-C, and the Control repair sustained 10 passes or less before the load cart test tire severely rutted the GP-GM cap.

Post-traffic inspection was performed carefully by digging trenches and removing the GP-GM with shovels to inspect the geocells. The control repair had the worst damage and was difficult to inspect. Most of the damage in the geocells for all repairs was at the upheaval near the location where the tire rutted the surface. The geocells were torn at the walls where perforations were located (Figure 6-2). It is possible that the GP-GM's larger/angular particles tore the geocells and that the cells stretched and tore when the tire punched through the GP-GM cap. Inspection of the first layer of geocells showed rutting, but the geocells were intact. Inspection of the CL subgrade also revealed rutting in all the repairs.

Figure 6-1. Damage after a few passes of trafficking the Phase 1 repairs.

(a) Repair 1-A after 13 passes.

(B) Control repair after 1 pass.

Although the repairs in Phase 1 sustained a limited number of passes, the results showed that repairs with geocell reinforcement performed better and that performance was improved with smaller geocell diameters. The results also showed that a thin GP-GM was not a suitable cap for contingency repairs and further proved that the performance of a pavement structure heavily relies on the subgrade strength (refer to Table 5-2). Since Repair 1-A

with the smallest geocell diameter showed better performance, the smaller cell openings were chosen for down-selection in Phase 2.

Figure 6-2. Damage to the 8-in.-height geocells in Repair 1-A after 13 passes.

6.2 Phase 2 repairs

Figure 6-3 shows a summary of the deformation measured throughout trafficking of the Phase 2 repairs. Trafficking on all repairs had to be halted after 3 in. of deformation was exceeded on the repairs with 8 in. and 16 in. of reinforcement. Excessive deformation in the repairs led to instability of the load cart and made it difficult to access the other two repairs. However, sufficient data had been collected on all repairs for analysis.

The rate of deformation at the repair with 8 in. of reinforcement was the highest, followed by the control (no geocell) repair. The repairs with 16 in. and 12 in. of reinforcement performed well and had similar rates of deformation. In general, 12 in. of reinforcement showed the best performance.

Post-traffic inspection of the repairs revealed cell wall buckling at the top and bottom layers of the 8-in.-thick geocells (Figure 6-4), where sand was displaced from adjacent cells and the wall bent. In all geocell-reinforced backfill repairs, cell penetration was observed, where the geocells pushed downward relative to the sand fill into the fabric membrane layer

underneath; however, no damage was observed in the geotextile. Posttest deformation measurements at each layer showed that the deformation at the surface of the CL subgrade was reduced as the thickness of reinforcement was increased, showing the effectiveness and impact of the geocells at distributing the applied load so as not to overstress the subgrade.

Figure 6-3. Deformation of Phase 2 repairs at different pass levels.

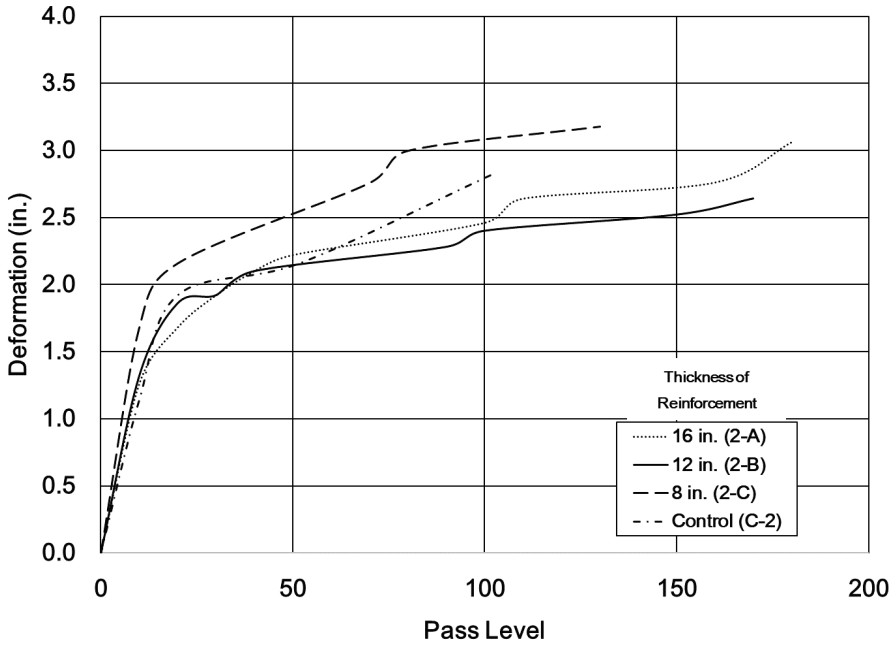

Figure 6-4. Buckling of the cell wall of the 8-in.-thick geocells after completion of Phase 2 trafficking.

6.3 Phase 3 repairs

A summary of the deformation measured throughout trafficking of the Phase 3 repairs is shown in Figure 6-5. Repair 3-D failed by rutting greater than 3 in. first and was followed by Repair 3-C. Repairs 3-A and 3-B were trafficked until 300 passes were completed, and both repairs reached 3 in. of rutting at that point. The rate of deformation was higher for Repairs 3-D and 3-C, although Repair 3-C, reinforced with Geoweb, was able to sustain at least 40 more passes before failure. The rate of deformation was similar for Repairs 3-A and 3-B, which were reinforced with Neoweb and EnviroGrid, respectively.

The results of this phase were used to relate the mechanical properties determined in the laboratory to performance, and it appeared that the trend in the field was similar to the trend in the lab. As discussed in Chapter 3, yield strength and breaking toughness for the Neoweb geocells were the highest, followed by EnviroGrid and then Geoweb geocells. While Neoweb and EnviroGrid yielded the best performance, the Geoweb product was chosen to continue testing in Phase 4 and Phase 5 to eliminate geocell type as a variable and to compare results to the prior phases of testing.

Figure 6-5. Deformation of Phase 3 repairs at different pass levels.

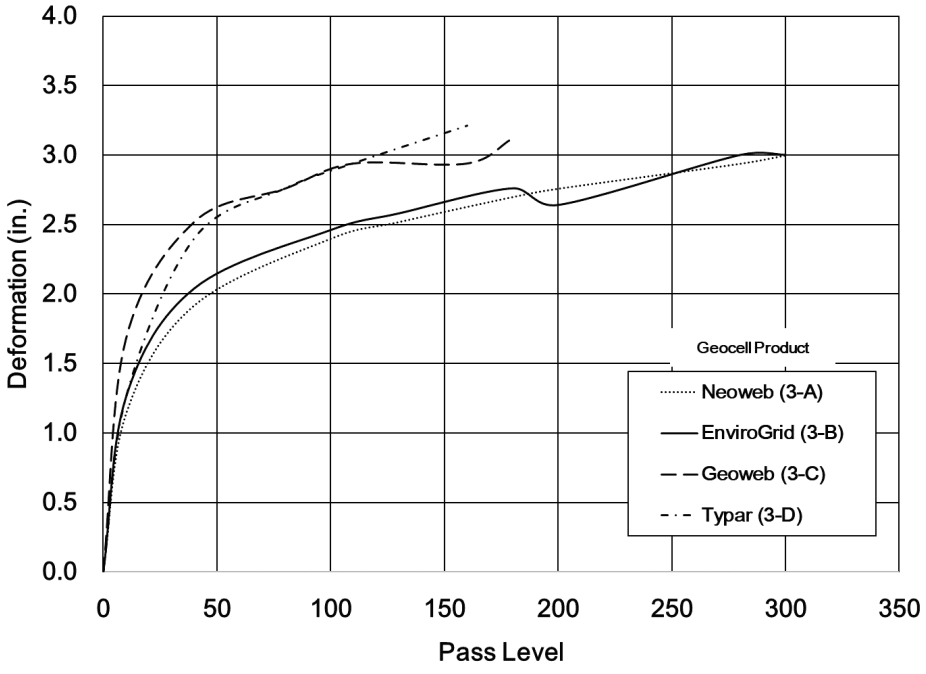

6.4 Phase 4 repairs

Figure 6-6 shows a summary of the deformation measured throughout trafficking of the Phase 4 repairs. Repairs 4-A (GP-GM), 4-B (SC with gravel), and 4-C (SP) were constructed and trafficked first. Thereafter, repairs 4-D (GW), 4-E (SC), and 4-F (CL-ML) were constructed and trafficked. The SC with gravel, SC, and GW backfill repairs appeared to have lower rates of deformation. The CL-ML backfill repair had the fastest rate of deformation, followed by the GP-GM and the SP repairs.

Trafficking was stopped before 3 in. of deformation was formed on the GW and SC backfill repairs because deformation data had been collected well above the minimum pass requirement of 100 passes, but all repairs reached at least 2.7 in. of deformation.

The CL-ML was the lowest quality material, and it was expected to fail before all the other backfill materials. The GP-GM was the highest quality material in this phase, but the repair with this backfill did not perform as well as expected. Posttest forensics revealed that the posttest CBRs on the CL subgrade of Repair 4-A (GP-GM) was 15 CBR (an increase of 6 CBR from the pretest CBR), while the CBR of the CL on both Repairs 4-B (SC w/ gravel) and 4-C (SP) was 25 CBR (an increase of at least 18 CBR from the pretest CBR.) This could explain the lower performance of the GP-GM and further reinforces the observation that the subgrade and foundation of a pavement structure play a key role in deformation performance.

Additionally, the CBR of the SC with gravel prior to trafficking was about 21 for the two geocell-reinforced layers. After trafficking was completed, the strength of the geocell-reinforced material had increased to 70 CBR on the bottom layer and 75 CBR on the top layer. The material dried out over time, yielding a reduction of about 2% moisture on the bottom layer and 1% moisture on the top layer. Once the material dried and hardened (i.e., natural cementation), it is hypothesized that the material properties, i.e., material strength, were the primary factor controlling performance; the geocells provided minimal additional strength to the system. All other repairs performed as expected.

Figure 6-6. Deformation of Phase 4 repairs at different pass levels.

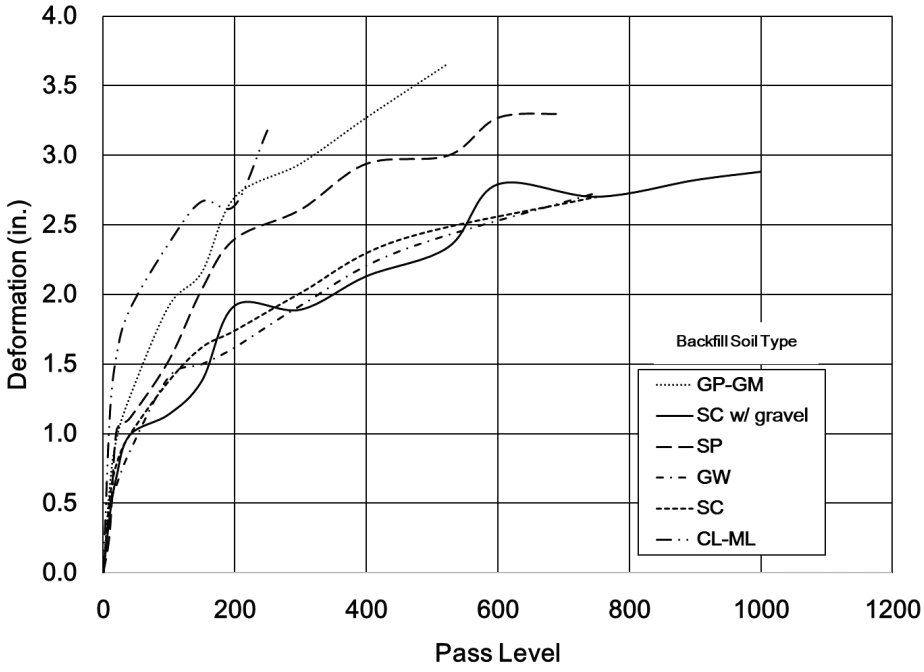

6.5 Phase 5 repairs

Since the 8-in.- and 6-in.-thick geocells both performed well in Phase 2 and had similar rates of deformation, additional testing was performed to eliminate the variable of the thickness of reinforcement and the height of the CL layer relative to the surface of the repair, i.e., the effect of the subgrade on overall rutting performance. Phase 5 aimed at specifically addressing the effect of geocell height on performance by making a relative comparison. The thickness of reinforcement was the same, but a different combination of layers was used.

Figure 6-7 shows a summary of the deformation measured throughout trafficking of the Phase 5 repairs. The rate of deformation for the repair with three layers of 8-in. geocells was higher than that of the repair with four layers of 6-in. geocells, where the latter sustained nearly twice the number of passes before failure. Similar rates of deformation were noted when compared to the Phase 2 repairs, which may be attributed to having moistures and densities closer to optimum in the Phase 2 repairs. Cell penetration was observed at all the layers, including the subgrade layer; however, no damage to the geotextile was observed. Posttest deformation

measurements at each layer showed that the deformation at the surface of the subgrade was similar for both repairs and remained under 1 in.

Figure 6-7. Deformation of Phase 5 repairs at different pass levels.

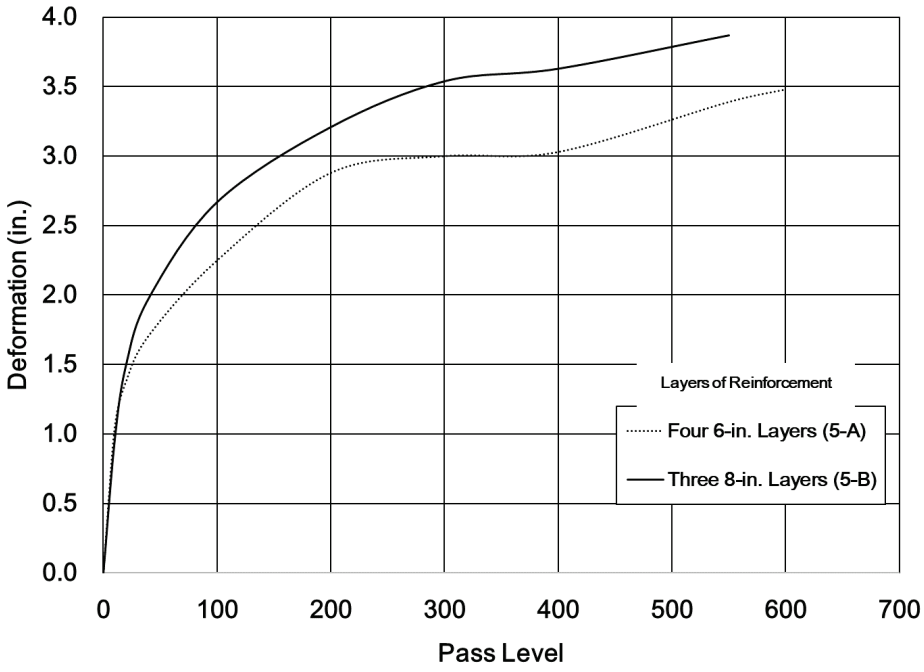

7 Conclusions and Recommendations

The report discussed the experimental program and results of laboratory-scale and full-scale testing of geocells and geocell-reinforced backfill pavement repairs. The project objectives were to perform (1) a market survey of traditional and new geocell products commercially available, (2) laboratory testing to characterize the different geocell materials and geometries, and (3) field experiments to characterize how geocell material, geometry, and various backfill soil types affect repair performance under simulated aircraft loads.

The project was conducted in a phased approach that started with a market survey, was followed by a laboratory characterization program, and ended with a full-scale testing program that assisted with down-selection of optimal geocell geometry and geocell material. Simulated repairs were built at the ERDC and trafficked with simulated aircraft loading; deformation was monitored to measure the performance of the repairs. The following are conclusions and recommendations based on the information discussed herein.

1. In general, geocells improved the load-deformation behavior of repairs through lateral confinement of the backfill material. The use of this technology to protect a weak subgrade continues to be more favorable than placing a low-quality backfill without reinforcement.
2. The optimal individual cell size was verified to be 8.8 in. x 10.2 in., according to the results of Phase 1. The smaller diameter ensures that there is geocell wall support provided relative to the size of the loaded area, i.e., relative to the size of the aircraft tire.
3. The optimal geocell heights are 8 in. (the height of the original product) and 6 in. Results from the Phase 2 and Phase 5 trafficking showed that an increase in the thickness of reinforcement provides increased protection to the subgrade, but there exists an optimum geocell thickness (6 in.) for protecting the subgrade. Better compaction can be achieved with thinner geocell layers, and the possibility of cell wall buckling is reduced with shorter geocell height. Based on these results, the 6-in.-thick geocells are also applicable for airfield pavement repairs and can be used as an alternative to the traditional 8-in.-thick geocells used in this application. This is favorable for procurement because the 6-in.-thick geocells tend to be more readily available and are less expensive.

4. The NPA and HDPE products appear to be the best-performing materials for this application and are recommended for procurement, provided that the correct geometry is chosen. The nonwoven geotextile geocell product is not recommended for this type of load support condition. The results of the laboratory testing of geocell material and mechanical properties appeared to mimic the geocell product performance in the field.
5. The benefit of geocell reinforcement is more appreciable when used in combination with low-quality soils, especially loose granular materials similar to concrete sand. Repair performance does not meaningfully benefit from the geocell reinforcement with high-quality materials or with fine materials that have high plasticity.
6. The use of smaller compaction equipment, such as a walk-behind vibratory plate compactor, rammer, and a vibratory drum compactor CTL attachment proved to achieve minimum compaction density requirements, provided that soils are placed near the optimum moisture content and the minimum amount of coverages are applied.
7. The experimental program for this project was designed around the assumption that geocells are intended for expedient repairs and temporary use. Recommendations for long-term use are beyond the scope of this report.

References

American Society for Testing and Materials International (ASTM). 2011a. *Standard test method for determining performance strength of geomembranes by the wide strip tensile method*. D4885-01(2011). West Conshohocken, PA: ASTM International.

_____. 2011b. *Standard test method for tensile properties of geotextiles by the wide-width strip method*. Designation: D4595-11. West Conshohocken, PA: ASTM International.

_____. 2012. *Standard test methods for laboratory compaction characteristics of soil using modified effort (56,000 ft-lbf/ft3 (2,700 kN-m/m3))*. Designation: D1557-12e. West Conshohocken, PA: ASTM International.

_____. 2014a. *Standard test method for deterioration of geotextiles by exposure to light, moisture and heat in a xenon arc type apparatus*. Designation D4355/D4355M-14. West Conshohocken, PA: ASTM International.

_____. 2014b. *Standard test method for determining the shear strength of soil-geosynthetic and geosynthetic-geosynthetic interfaces by direct shear*. Designation: D5321/D5321M-14. West Conshohocken, PA: ASTM International.

_____. 2014c. *Standard test methods for specific gravity of soil solids by water pycnometer*. Designation D854-14. West Conshohocken, PA: ASTM International.

_____. 2015. *Standard test method for density and unit weight of soil in place by sand-cone method*. Designation: D1556/D1556M-15e1. West Conshohocken, PA: ASTM International.

_____. 2016a. *Standard test method for California Bearing Ratio (CBR) of laboratory-compacted soils*. Designation: D1883-16. West Conshohocken, PA: ASTM International.

_____. 2016b. *Standard test method for nonrepetitive static plate load tests of soils and flexible pavement components, for use in evaluation and design of airport and highway pavements*. Designation: D1196/D1196M-12. West Conshohocken, PA: ASTM International.

_____. 2017a. *Standard practice for classification of soils for engineering purposes (Unified Soil Classification system)*. Designation: D2487-17e1. West Conshohocken, PA: ASTM International.

_____. 2017b. *Standard test methods for in-place density and water content of soil and soil-aggregate by nuclear methods (shallow depth)*. Designation: D6938-17a. West Conshohocken, PA: ASTM International.

_____. 2018. *Standard test method for use of the dynamic cone penetrometer in shallow pavement applications*. Designation: D6951/D6951M-18. West Conshohocken, PA: ASTM International.

_____. 2019. *Standard test methods for laboratory determination of water (moisture) content of soil and rock by mass*. Designation: D2216-19. West Conshohocken, PA: ASTM International.

Bell, H. P., L. Edwards, W. D. Carruth, J. S. Tingle, and J. R. Griffin. 2013. *Wet weather crater repair testing at Silver Flag Exercise Site, Tyndall Air Force Base, Florida*. ERDC/GSL TR-13-42. Vicksburg, MS: U.S. Army Engineer Research and Development Center.

Carruth, W. D., L. Edwards, H. P. Bell, J. S. Tingle, J. R. Griffin, and C. A. Rutland. 2015. *Large crater repair at Silver Flag Exercise Site, Tyndall Air Force Base, Florida*. ERDC/GSL TR-15-27. Vicksburg, MS: U.S. Army Engineer Research and Development Center.

Department of Defense. 2002. *Airfield damage repair*. United Facilities Criteria (UFC) 3-270-07. Washington, DC: U.S. Army Corps of Engineers (USACE), Naval Facilities Engineering Command (NAVFAC) and U. S. Air Force Civil Engineering Center (AFCEC).

Edwards, L., H. P. Bell, W. D. Carruth, J. R. Griffin, and J. S. Tingle. 2013. *Cold weather crater repair testing at Malmstrom Air Force Base, Montana*. ERDC/GSL TR-13-32. Vicksburg, MS: U.S. Army Engineer Research and Development Center.

International Organization for Standardization. 2003. *Geotextiles and geotextile-related products — strength of internal structural junctions — part 1: geocells*. ISO 13426-1. Switzerland: International Organization for Standardization.

Priddy, L. P., J. S. Tingle, M. C. Edwards, J. R. Griffin, and T. J. McCaffrey. 2013. *CRATR technology demonstration: limited operational utility assessment 2, Tyndall Air Force Base, Florida*. ERDC/GSL TR-13-39. Vicksburg, MS: U.S. Army Engineer Research and Development Center.

Read, D. L., and P. E. Dukes. 1988. *Sand grid base course phase I, for fiberglass mat crater repair*. RRR-TR-88-01. Tyndall Air Force Base, FL: Air Force Engineering and Services Center.

Rushing, T. M., W. C. Floyd, L. Garcia, and Q. S. Mason. 2016. *Development of an air-droppable airfield damage repair kit*. ERDC/GSL TR-16-25. Vicksburg, MS: U.S. Army Engineer Research and Development Center.

Tingle, J. S., L. P. Priddy, M. C. Edwards, C. A. Gartrell, and T. J. McCaffrey. 2009. *Critical runway assessment and repair (CRATR) technology demonstration: limited operational utility assessment 1 (LOUA1), Tyndall Air Force Base, Florida*. ERDC/GSL TR-09-12. Vicksburg, MS: U.S. Army Engineer Research and Development Center.

United States Air Force (USAF). 1992. *Crushed-stone crater repair and line-of-sight profile measurement for rapid runway repair*. TO 35E2-5-1. Washington, DC: USAF.

U.S. Army Corps of Engineers (USACE). 1995. *Standard test method for determining the modulus of soil reaction. Handbook for concrete and cement*. CDC-C 655-95. Washington, DC: U.S. Army Corps of Engineers.

Webster, S. L. 1979. *Investigation of beach sand trafficability enhancement using sand-grid confinement and membrane reinforcement concepts: sand test sections 1 and 2. Report 1*. Vol. 79, No. 20. Vicksburg, MS: U.S. Army Engineer Waterways Experiment Station.

_____. 1981. *Investigation of beach sand trafficability enhancement using sand-grid confinement and membrane reinforcement concepts. Report 2. Sand test sections 3 and 4*. WES/TR/GL-79-20. Vicksburg, MS: U.S. Army Engineer Waterways Experiment Station.

_____. 1984. *Sand-grid demonstration road constructed at Fort Story, Virginia*. Information Exchange Bulletin. Vol O-84-1. Vicksburg, MS: U.S. Army Engineer Waterways Experiment Station.

_____. 1986. *Sand-grid demonstration roads constructed for JLOTS II tests at Fort Story, Virginia*. No. GL-86-19. Vicksburg, MS: U.S. Army Engineer Waterways Experiment Station.

Webster, S. L., and S. J. Alford. 1978. *Investigation of construction concepts for pavements across soft ground*. WES TR-S-78-6. Vicksburg, MS: U.S. Army Engineer Waterways Experiment Station.

Appendix A

This appendix shows the results of ASTM D 5321: Standard Test Method for Determining the Shear Strength of Soil-Geosynthetic and Geosynthetic-Geosynthetic Interfaces by Direct Shear (2014b).

Figure A1. Results for Presto – Geoweb.

Ottowa Sand, 20-30 vs.
Geocell - HDPE-A-8 Presto HDPE

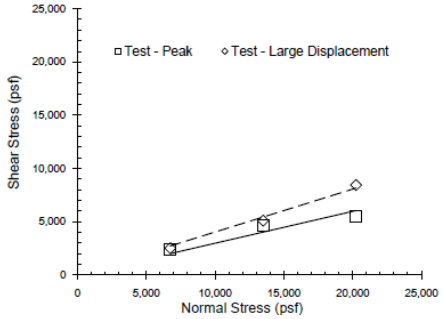

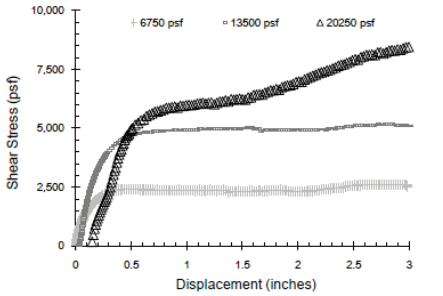

Test Results, Linear Regression			
Mohr-Coulomb Parameters		Inflection	Large Displacement
Friction Angle	Degrees	16.6	21.9
Y-intercept or Adhesion	psf	0 (Forced)	0 (Forced)
Minimum Secant Angle	Degrees	15.2	20.5

Note - Large Displacement Values Reported for 3.0 inches of Displacement

Test Conditions		
Upper Box	Ottowa Sand, 20-30	
Lower Box	Geocell - HDPE-A-8 Presto HDPE	
Conditioning	Wet - Loading applied and Interface flooded for a minimum of 15 minutes prior to shear.	
Shearing Rate	inches/minute	0.04

Test Notes
Shearing occurred at the interface at all stresses.

Specimen No.		-	1	2	3
Normal Stress		psf	6,750	13,500	20,250
Box Edge Dimension		in	12	12	8
Bearing Slide Resistance		lbs	72	136	94
Inflection / First Peak	Shear Stress	psf	2,367	4,640	5,516
	Secant Angle	deg.	19.3	19.0	15.2
Large Displacement	Shear Stress	psf	2,524	5,101	8,446
	Secant Angle	deg.	20.5	20.7	22.6

Figure A2. Results for PRS Geo-technologies – Neoweb.

Ottowa Sand, 20-30 vs.
Geocell - NPA-8 PRS Novel Polymer Alloy

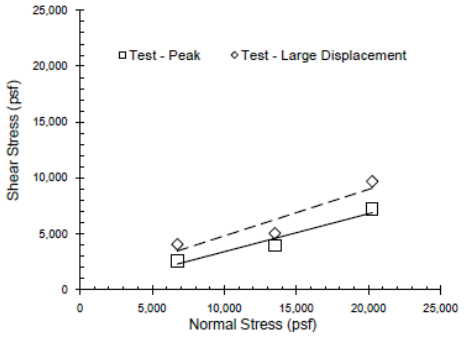

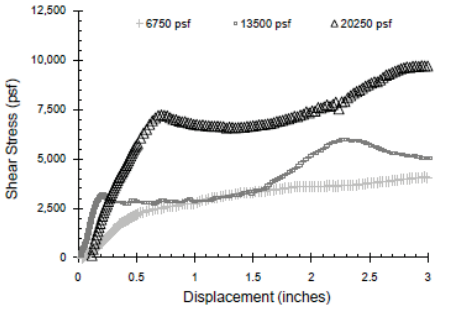

Test Results, Linear Regression			
Mohr-Coulomb Parameters		Inflection	Large Displacement
Friction Angle	Degrees	18.8	22.6
Y-intercept or Adhesion	psf	0 (Forced)	637
Minimum Secant Angle	Degrees	16.4	20.5

Note - Large Displacement Values Reported for 3.0 inches of Displacement

Test Conditions		
Upper Box	Ottowa Sand, 20-30	
Lower Box	Geocell - NPA-8 PRS Novel Polymer Alloy	
Conditioning	Wet - Loading applied and Interface flooded for a minimum of 15 minutes prior to shear.	
Shearing Rate	inches/minute	0.04

Test Notes
Shearing occurred at the interface at all stresses.

Specimen No.		-	1	2	3
Normal Stress		psf	6,750	13,500	20,250
Box Edge Dimension		in	12	12	8
Bearing Slide Resistance		lbs	72	136	94
Inflection / First Peak	Shear Stress	psf	2,574	3,980	7,218
	Secant Angle	deg.	20.9	16.4	19.6
Large Displacement	Shear Stress	psf	4,065	5,046	9,697
	Secant Angle	deg.	31.1	20.5	25.6

Figure A3. Results for Geo Products – EnviroGrid.

Ottowa Sand, 20-30 vs.
Geocell - HDPE-B8 Envirogrid HDPE

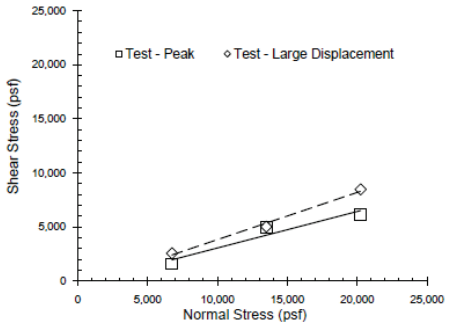

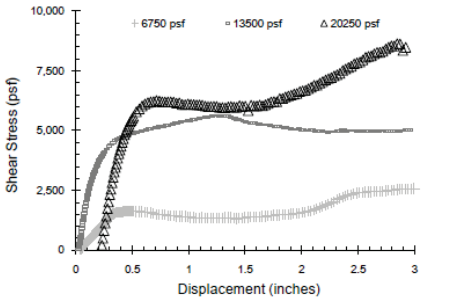

Test Results, Linear Regression			
Mohr-Coulomb Parameters		Inflection	Large Displacement
Friction Angle	Degrees	17.6	21.9
Y-intercept or Adhesion	psf	0 (Forced)	0 (Forced)
Minimum Secant Angle	Degrees	13.3	20.4

Note - Large Displacement Values Reported for 3.0 inches of Displacement

Test Conditions		
Upper Box	Ottowa Sand, 20-30	
Lower Box	Geocell - HDPE-B8 Envirogrid HDPE	
Conditioning	Wet - Loading applied and Interface flooded for a minimum of 15 minutes prior to shear.	
Shearing Rate	inches/minute	0.04

Test Notes
Shearing occurred at the interface at all stresses.

Specimen No.		-	1	2	3
Normal Stress		psf	6,750	13,500	20,250
Box Edge Dimension		in	12	12	8
Bearing Slide Resistance		lbs	72	136	94
Inflection / First Peak	Shear Stress	psf	1,600	4,961	6,170
	Secant Angle	deg.	13.3	20.2	16.9
Large Displacement	Shear Stress	psf	2,576	5,034	8,478
	Secant Angle	deg.	20.9	20.4	22.7

Figure A4. Results for Typar – GeoCell GS.

Ottowa Sand, 20-30 vs.
Geocell - NW-8 Non-woven PP/PE

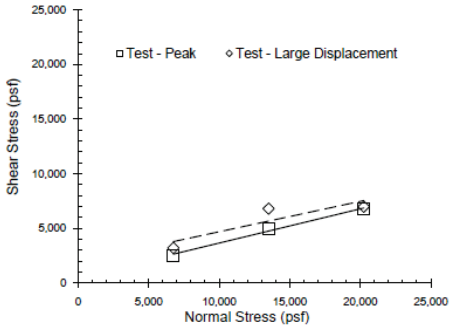

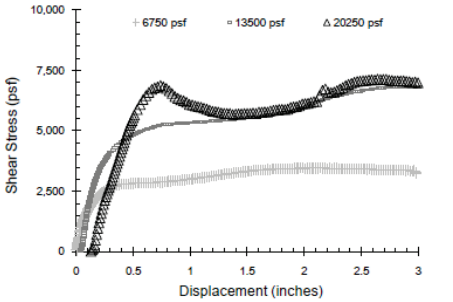

Test Results, Linear Regression			
Mohr-Coulomb Parameters		Inflection	Large Displacement
Friction Angle	Degrees	17.4	15.6
Y-intercept or Adhesion	psf	515	1,907
Minimum Secant Angle	Degrees	18.5	19.0

Note - Large Displacement Values Reported for 3.0 inches of Displacement

Test Conditions		
Upper Box	Ottowa Sand, 20-30	
Lower Box	Geocell - NW-8 Non-woven PP/PE	
Conditioning	Wet - Loading applied and Interface flooded for a minimum of 15 minutes prior to shear.	
Shearing Rate	inches/minute	0.04

Test Notes
Shearing occurred at the interface at all stresses.

Specimen No.		-	1	2	3
Normal Stress		psf	6,750	13,500	20,250
Box Edge Dimension		in	12	12	8
Bearing Slide Resistance		lbs	72	136	94
Inflection / First Peak	Shear Stress	psf	2,542	4,935	6,779
	Secant Angle	deg.	20.6	20.1	18.5
Large Displacement	Shear Stress	psf	3,222	6,808	6,987
	Secant Angle	deg.	25.5	26.8	19.0

Appendix B

This appendix shows the grain-size distribution curves for the soils used throughout testing, including SP, CL, GP-GM, SC, GW, and ML.

Figure B1. Grain-size distribution for SP.

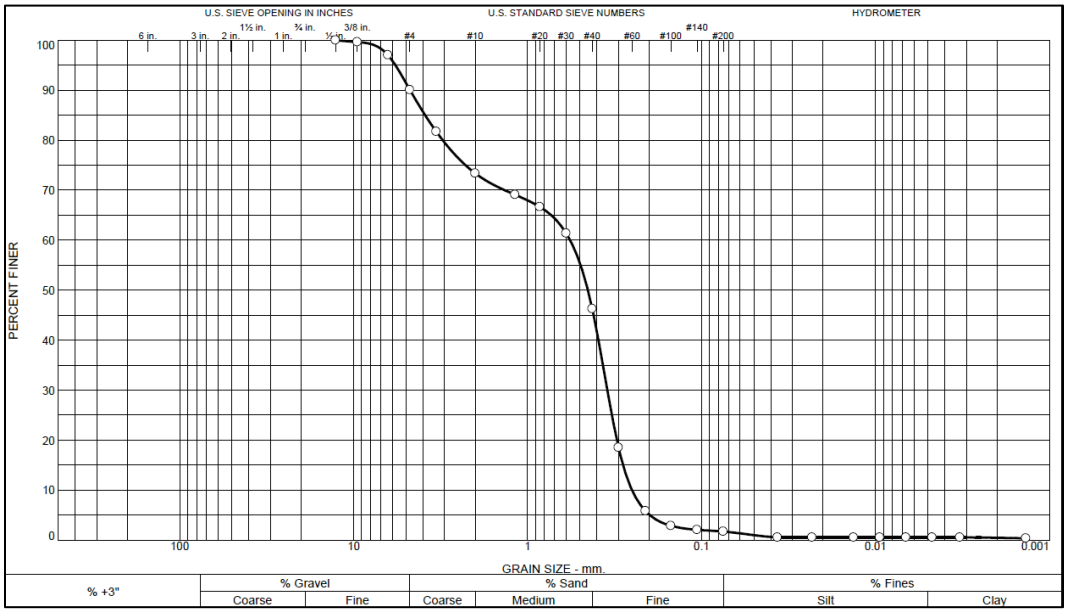

Figure B2. Grain-size distribution for CL.

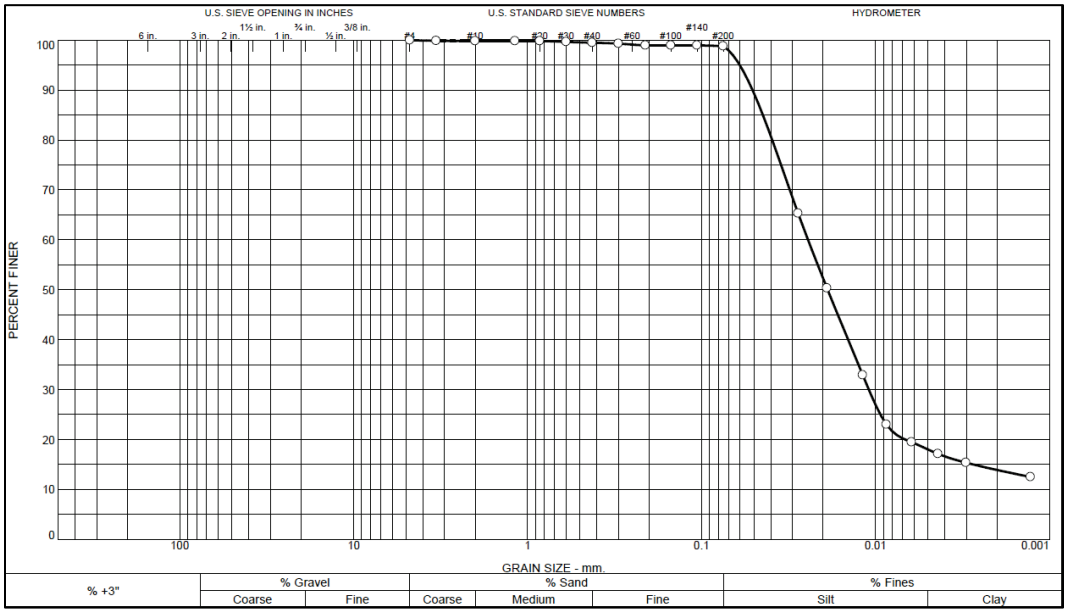

Figure B3. Grain-size distribution for GP-GM.

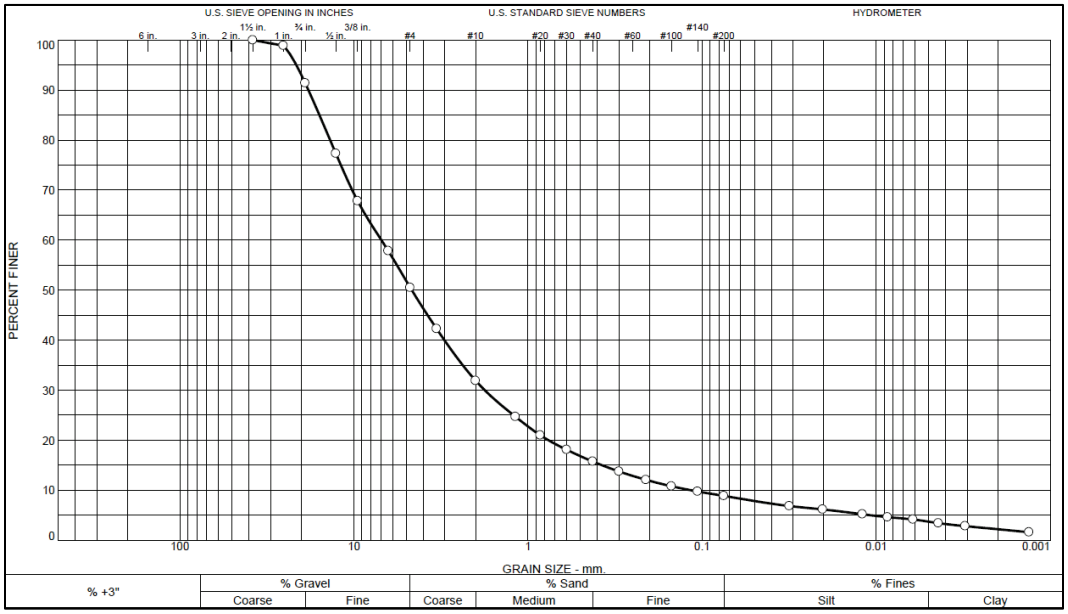

Figure B4. Grain-size distribution for clayey sand with gravel (SC).

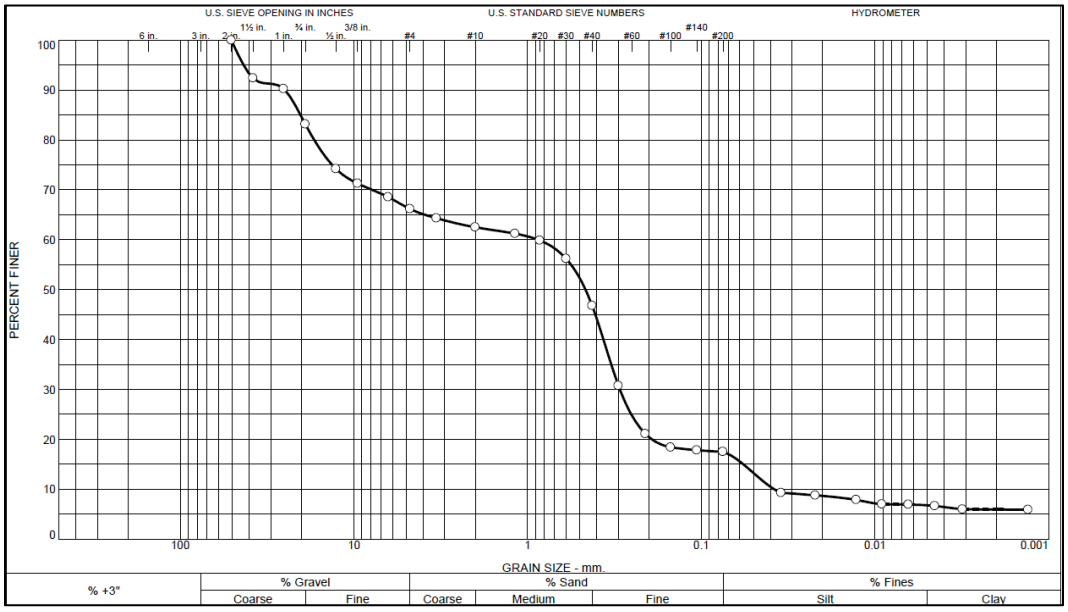

Figure B5. Grain-size distribution for clayey sand (SC).

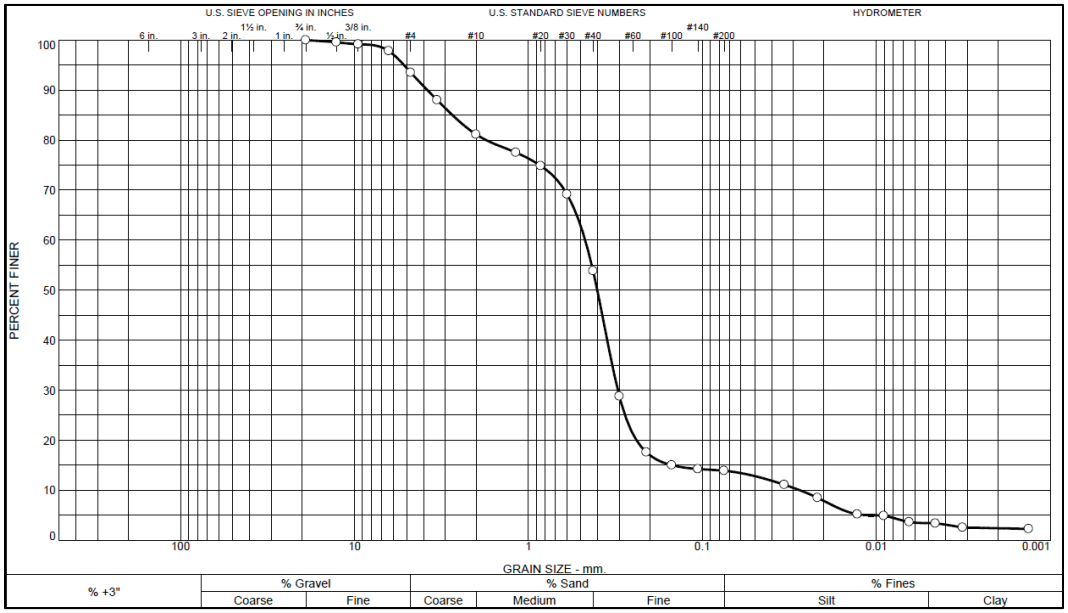

Figure B6. Grain-size distribution for GW.

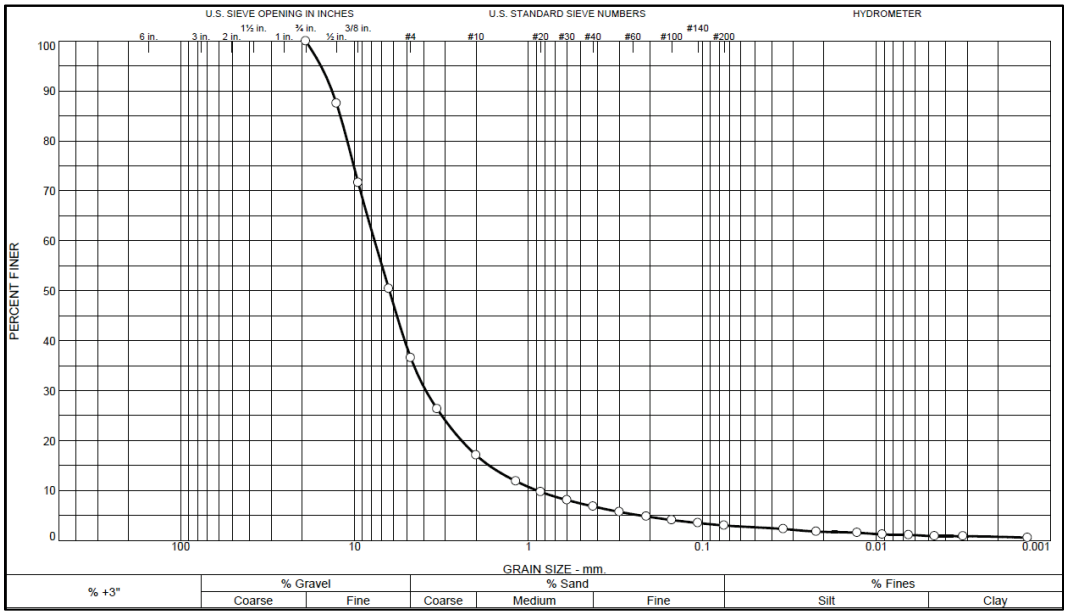

Figure B7. Grain-size distribution for ML.

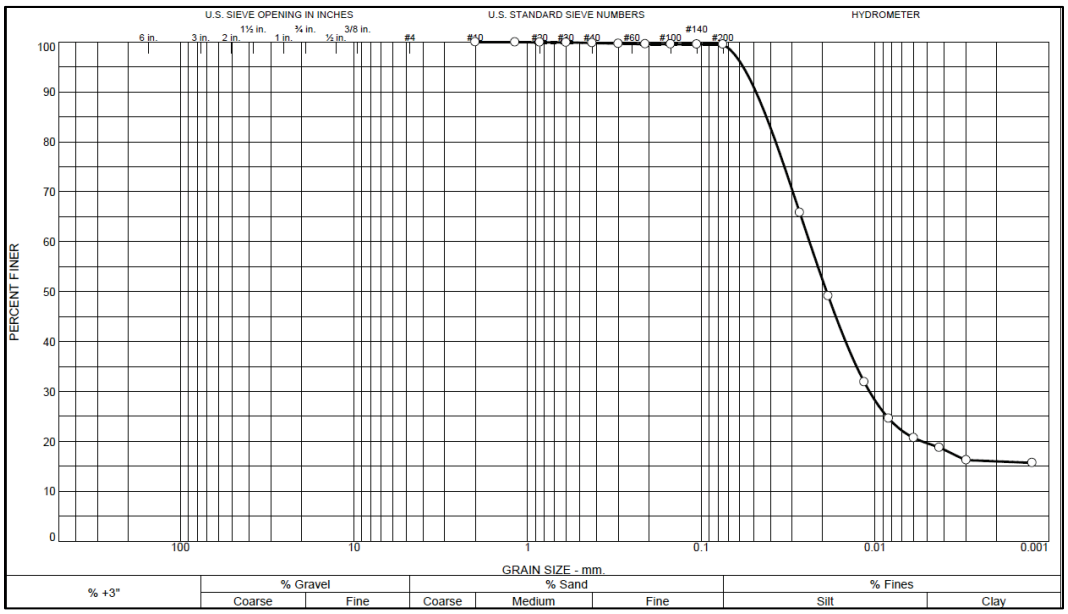

Acronyms and Abbreviations

ADR	Airfield Damage Repair
ASTM	American Society for Testing and Materials
CBR	California Bearing Ratio
Cc	Coefficient of curvature
CL	Low-Plasticity Clay
CL-ML	Silty Clay
CRATR	Critical Runway Assessment Repair
Cu	Uniformity coefficient
DCP	Dynamic Cone Penetrometer
ERDC	Engineer Research and Development Center
FOD	Foreign Object Debris
FRP	Fiberglass-Reinforced Polymer
GP-GM	Poorly Graded Gravel with Silty Sand
GW	Well-Graded Sand
HDPE	High-Density Polyethylene
JCTD	Joint Capabilities Technology Demonstration
LL	Liquid limit
MC	Moisture Content
NPA	Novel Polymeric Alloy
NW	Non-woven
OUA	Operational Utility Assessment
PCC	Portland Concrete Cement
PI	Plasticity index
RADR	Rapid Airfield Damage Recovery
SC	Clayey Sand
SP	Poorly Graded Sand
TTPs	Tactics, Techniques, and Procedures
UFC	United Facilities Criteria
WD	Wet Density

REPORT DOCUMENTATION PAGE

Form Approved
OMB No. 0704-0188

1. REPORT DATE *(DD-MM-YYYY)*	2. REPORT TYPE	3. DATES COVERED *(From - To)*
December 2021	Final	

4. TITLE AND SUBTITLE

Rapid Airfield Damage Recovery Program;

Evaluation of Geocell-Reinforced Backfill for Airfield Pavement Repair

5a. CONTRACT NUMBER

5b. GRANT NUMBER

5c. PROGRAM ELEMENT NUMBER

6. AUTHOR(S)

Lyan Garcia, Jay Rowland, and Jeb Tingle

5d. PROJECT NUMBER
475573

5e. TASK NUMBER

5f. WORK UNIT NUMBER

7. PERFORMING ORGANIZATION NAME(S) AND ADDRESS(ES)

Geotechnical and Structures Laboratory
U.S. Army Engineer Research and Development Center
3909 Halls Ferry Road
Vicksburg, MS 39180-6199

8. PERFORMING ORGANIZATION REPORT NUMBER

ERDC/GSL TR-21-41

9. SPONSORING / MONITORING AGENCY NAME(S) AND ADDRESS(ES)

Air Force Civil Engineer Center
Panama City, FL 32403

10. SPONSOR/MONITOR'S ACRONYM(S)

11. SPONSOR/MONITOR'S REPORT NUMBER(S)

12. DISTRIBUTION / AVAILABILITY STATEMENT

Approved for public release: distribution unlimited.

13. SUPPLEMENTARY NOTES

Geocell TTP Refinement

14. ABSTRACT

After an airfield has been attacked, temporary airfield pavement repairs should be accomplished quickly to restore flight operations. Often, the repairs are made with inadequate materials and manpower due to limited available resources. Legacy airfield damage repair (ADR) methods for repairing bomb damage consist of using debris to fill the crater, followed by placement of crushed stone or rapid-setting flowable fill backfill with a foreign object debris (FOD) cover. While these backfill methods have provided successful results, they are also heavily dependent on specific material and equipment resources that are not always readily available. Under emergency conditions, it is desirable to reduce the logistical burden while providing a suitable repair, especially in areas with weak subgrades. Geocells are cellular confinement systems of interconnected cells that can be used to reinforce geotechnical materials. The primary benefit of geocells is that lower quality backfill materials can be used instead of crushed stone to provide a temporary repair. This report summarizes a series of laboratory and field experiments performed to evaluate different geocell materials and geometries in combinations with a variety of soils to verify their effectiveness at supporting heavy aircraft loads. Results provide specific recommendations for using geocell technology for backfill reinforcement for emergency airfield repairs.

15. SUBJECT TERMS

Sand grid
Geocells
Military bases
Airfield damage repair
Soil reinforcement
Geosynthetics
Geogrids
Runways (Aeronautics)—Maintenance and repair
Controlled low-strength materials
Fills (Earthwork)

16. SECURITY CLASSIFICATION OF:			17. LIMITATION OF ABSTRACT	18. NUMBER OF PAGES	19a. NAME OF RESPONSIBLE PERSON
a. REPORT	b. ABSTRACT	c. THIS PAGE			19b. TELEPHONE NUMBER *(include area code)*
Unclassified	Unclassified	Unclassified	SAR	79	